

Multi-GPU MBE(3)-OSV-MP2 for Performant Large-Scale *ab initio* Calculations

Qiujiang Liang^{†,‡} and Jun Yang^{*,†,‡,¶}

[†]*Department of Chemistry, The University of Hong Kong, Hong Kong 999077, P.R. China*

[‡]*Hong Kong Quantum AI Lab Limited, Hong Kong 999077, P.R. China*

[¶]*CAS-HKU Joint Laboratory on New Materials, The University of Hong Kong, Hong Kong 999077, P.R. China*

E-mail: juny@hku.hk

Abstract

The computational acceleration of orbital-invariant local correlation methods on graphics processing units (GPUs) has remained largely unexplored due to substantial algorithmic complexities. The runtime efficiency of GPU-implemented local correlation theories can be significantly constrained by the parallelizable degree of the orbital localization procedure, the iterative solution of the local wave function, and the adaptation of CUDA kernels to inherently local or sparse operations. Using the second-order Møller-Plesset perturbation (MP2) theory, we present a multi-GPU implementation for large-scale third-order many-body expansion orbital-specific virtual MP2 (MBE(3)-OSV-MP2) energy calculations. Accordingly, our algorithms and implementation address the GPU parallelization ability for peak utilization and parallelism of local MP2 computation in several aspects, including Jacobi-Pipek-Mezey localization, randomized OSV generation, direct MP2 integral regeneration, as well as CUDA kernel adaptation to local operations. The GPU-based MBE(3)-OSV-MP2 energy computation achieves $\mathcal{O}(N^{1.9})$ scaling and 84% parallel efficiency up to 24 GPUs distributed on multiple

nodes. The present implementation delivers 40-fold wall-time speedup of the canonical RI-MP2 and 10-fold speedup of the CPU-based MBE(3)-OSV-MP2 for $(\text{H}_2\text{O})_{128}/\text{cc-pVDZ}$ and $(\text{H}_2\text{O})_{190}/\text{cc-pVDZ}$, respectively. A large scale computation of 784-atom insulin peptide yields the full MBE(3)-OSV-MP2 energies in 24 minutes with cc-pVDZ (7571 basis functions) and 6.4 hours with cc-pVTZ (17448 basis functions) on 8 NVIDIA A800 GPUs. Our work opens up new possibilities for performing fast GPU-based local correlation calculations on real-life macromolecules.

1 Introduction

Accurate *ab initio* electronic structure prediction of macromolecules is computationally intensive and requires tremendous computing time and resources, as compared to classical computation. Significant advancements have been made in the past decade to extend the applicability and efficiency of post-Hartree-Fock calculations that provide systematically controllable accuracy. Second-order Møller-Plesset perturbation theory (MP2) is the simplest wave function-based method, but of high importance in computational chemistry and materials, as it captures a large portion of the correlation energy as well as covalent, ionic, and van der Waals interactions more accurately than many popular density functional theory (DFT) approximations. The MP2 correlation energy is an essential component of the fifth-rung double-hybrid functionals,^{1,2} which helps make one of the most robust and accurate DFT approaches. MP2 presently offers the most practical wave function method to optimize geometries of large main group compounds.³⁻⁸ It is now feasible to apply MP2 to describe dynamic electron correlations in rather complex systems,⁹⁻¹³ up to benchmark demonstrations for biological structure¹⁴ and liquid¹⁵ of tens to hundreds of thousands of atoms. These developments have been largely driven by implementing novel MP2 methods that reduce the steep $\mathcal{O}(N^5)$ scaling (N : molecular size) and that enable massive parallelization on modern computing platforms including central processing units (CPUs) and graphics processing units (GPUs).

There have been many MP2 reformulations aiming to overcome the canonical $\mathcal{O}(N^5)$ barrier. The Laplace-transformed MP2 computes the canonical correlation energy on $\mathcal{O}(N^4)$ by con-

tracting molecular orbital (MO) indices to Laplace integration variables implemented for both molecules¹⁶ and solids,¹⁷ and the relevant linear scaling models have been also developed.^{10,18,19} The Scaled-Opposite-Spin MP2 (SOS-MP2) gives similar $\mathcal{O}(N^4)$ using Laplace transformation²⁰ and even lower $\mathcal{O}(N^3)$ using atomic orbitals.²¹ Another important domain of the scaling-reduced MP2 is a range of local correlation methods that exploit the locality of electrons^{22,23} in both occupied and virtual local MOs. A variety of local full-system MP2 ansätze has been defined to select a subset of compact cluster operators in different ways^{10,24–29} that are also mutually related. Moreover, a bottom-up fragmentation approach attempts to solve many smaller MP2 equations of the molecular fragments and synthesize these sub-system solutions to approximate the super-system.^{8,11,14,15,30–34} In particular, by combining the best of both streams, the present authors have developed a third-order many-body expansion of the wave function amplitudes in an orbital-specific-virtual MP2, coined MBE(3)-OSV-MP2,⁸ to reduce the scalings in occupied and virtual LMOs. The resulting MBE(3)-OSV-MP2 energy and analytical gradient computations achieve $\mathcal{O}(N^2)$ and $\mathcal{O}(N^{2\sim 3})$ costs,⁸ respectively. The ability of these algorithms for reducing the $\mathcal{O}(N^5)$ complexity emerges at a manageable balance with the exactness of MP2 correlation energy, achieving about 10–100× speedups.

Canonical and scaling-reduced MP2 models compute at various $c\mathcal{O}(N^x)$ ($x \approx 1 - 5$; c : prefactor) scalings. For large molecules, multiple $\mathcal{O}(N^x)$ throughputs are invoked, resulting in significant prefactors c , which is another crucial source of computational bottlenecks besides the formal scaling. For enabling enormous acceleration of MP2 simulations of chemically and biologically relevant macromolecules, the large prefactor c must be mitigated using accelerators. With the advent of modern terascale high-performance computing platforms, such as the widely used CPUs and GPUs, efficient parallel computational designs are spurred and have been implemented to simultaneously execute MP2 $\mathcal{O}(N^x)$ tasks. In recent decades, GPU-based computations are gaining substantial improvements and increasing popularity for quantum chemistry, as compared to CPU-only computation. The high GPU memory bandwidth and large-scale floating-point throughput enable superior linear algebra operations by launching thousands of threads simultaneously. How-

ever, this unique GPU architecture necessitates entirely new designs and optimizations for all major computational steps in Hartree-Fock and MP2: Paramount advancements in the past have been made to enhance GPU parallel efficiencies for four-center electron repulsion integrals (ERIs),³⁵⁻⁴² three-center density fitting (DF) integrals,^{13,40,43,44} two-center hypercontraction integrals,^{45,46} Fock construction,^{39,44,47-50} canonical MP2,⁵¹⁻⁵³ DF-MP2,^{13,14,54-57} and SOS-MP2 models.^{21,45,46}

The GPU-enabled local MP2 correlation calculations are still largely limited to fragmentation methods.^{12,58,58-61} Each fragment’s DF-MP2 can be ported to GPUs to allow massive parallelization, and the aforementioned molecular GPU-enabled DF-MP2 parallelisms are readily available for implementing fragmentation MP2. However, the local correlation approximation to the entire system wave function introduces additional complexities compared to canonical DF-MP2 on GPUs. Firstly, the localization of occupied and virtual MOs involves an overall $\mathcal{O}(N^3)$ - $\mathcal{O}(N^4)$ scaling, which quickly becomes formidably intensive and a significant bottleneck, thereby elevating the overall scaling of local MP2 for large molecules. The parallel scalability of the localization function is poor when the number of parallel processes increases. Second, the Fock matrix in the LMO representation contains significant off-diagonal elements, leading to an iterative procedure where coupled residual equations must be solved for local MP2 amplitudes and energies. This poses a significant challenge to maintaining data transmission balance and memory management within the GPU architecture. Finally, the local MP2 is represented in compact orbital spaces and relies heavily on linear algebra operations for processing many small matrices. These operations are inherently latency- and memory-bound on GPUs, resulting in a considerable degradation in the performance of NVIDIA’s `cuBLAS` and `cuSolver` libraries when launching these library functions to execute such high-throughput small operations.

This work tackles these critical issues by employing our previously developed MBE(3)-OSV-MP2 local correlation model. We adopted a fully integral-direct generator for MP2 half-transformed 3c2e coefficients, making use of high GPU memory bandwidth and floating point operations to avoid excessive I/O overheads. Additionally, we implemented the following localization methods on GPU thread blocks: the Pipek-Mezey (PM) localization algorithm using Jacobi pairwise orbital

rotations⁶² for preparing occupied LMOs at $\mathcal{O}(N^2)$ scaling, and the randomized diagonalization scheme for preparing virtual LMOs (i.e., OSVs) at sub-quadratic scaling. Moreover, we developed custom CUDA kernel functions to implement linear algebra transformations as needed throughout the OSV construction, OSV integrals and OSV-MP2 residual equations.

This paper is structured as follows. Section 2 provides an overview of the notation and theory behind the MBE(3)-OSV-MP2 method. Section 3 presents our detailed algorithms and GPU implementation for key steps in local MP2 calculations, including orbital localization, OSV generation, computation of local OSV-MP2 intermediates and residual equations. Section 4 presents benchmark results and illustrative applications to demonstrate the GPU’s run-time efficiency and parallel capabilities for large molecules. Section 5 summarizes this work.

2 MBE(3)-OSV-MP2 Method

We present a concise overview of the MBE(3)-OSV-MP2,⁸ adopting the following orbital notation convention: i, j, k, \dots denote occupied molecular orbitals (MOs), either canonical or localized (LMOs), while a, b, c, \dots represent canonical virtual MOs. The indices $\bar{\mu}_k, \bar{\nu}_k, \bar{\xi}_k, \dots$ indicate OSVs associated with the occupied LMO k . The indices p, q, r, \dots and α, β, \dots refer to generic MOs and atomic orbitals (AOs), respectively. The auxiliary fitting AOs are denoted by A, B, \dots . The matrix trace operation is expressed using bra-ket notation $\langle \dots \rangle$. Tensors and matrices are denoted in boldface, with their elements in italics.

For closed-shell systems, the canonical MP2 wave function amplitudes \mathbf{T}_{ij} are composed of elements by

$$T_{ij}^{ab} = \frac{K_{ij}^{ab}}{f_{ii} + f_{jj} - f_{aa} - f_{bb}}, \quad (1)$$

where f_{pp} denotes the diagonal elements of the Fock matrix and $K_{ij}^{ab} = (ia|jb)$ the MP2 exchange integral. However, the local OSV-MP2 correlation amplitudes must be solved iteratively in a set of

nonlinear residual equations $\mathbf{R}_{(ij,ij)}$,

$$\begin{aligned} \mathbf{R}_{(ij,ij)} = & \mathbf{K}_{(ij,ij)} + \sum_k \left\{ \mathbf{S}_{(ij,ik)} \mathbf{T}_{(ik,ik)} [\delta_{kj} \mathbf{F}_{(ik,ij)} - f_{kj} \mathbf{S}_{(ik,ij)}] \right. \\ & \left. + [\delta_{ik} \mathbf{F}_{(ij,kj)} - f_{ik} \mathbf{S}_{(ij,kj)}] \mathbf{T}_{(kj,kj)} \mathbf{S}_{(kj,ij)} \right\}, \end{aligned} \quad (2)$$

and thus minimize the Hylleraas energy functional for orbital invariance. Above, all needed matrices in the form of $\mathbf{A}_{(ij,kl)}$ are formulated in the OSV basis \mathbf{Q}_i for an LMO i . The OSV basis diagonalizes the semi-canonical MP2 diagonal amplitudes (\mathbf{T}_{ii}),

$$\left[\mathbf{Q}_i^\dagger \mathbf{T}_{ii} \mathbf{Q}_i \right]_{\bar{\mu}_i \bar{\nu}_i} = \omega_{\bar{\mu}_i} \delta_{\bar{\mu}_i \bar{\nu}_i}, \quad (3)$$

with the orthonormality condition $\mathbf{Q}_i^\dagger \mathbf{Q}_i = \mathbf{1}$. The eigenvalues $\omega_{\bar{\mu}_i}$ reflect the importance of the corresponding OSV space, allowing selection of OSVs based on a truncation parameter l_{osv} . In eq 2, $\mathbf{A}_{(ij,kl)}$ generally represents a 4-block full OSV-based matrix including submatrices corresponding to direct excitation ($i \rightarrow \bar{\mu}_i$) and exchange excitation ($i \rightarrow \bar{\nu}_j$),

$$\mathbf{A}_{(ij,kl)} = \begin{pmatrix} \mathbf{Q}_i^\dagger \\ \mathbf{Q}_j^\dagger \end{pmatrix} \mathbf{A} \begin{pmatrix} \mathbf{Q}_k & \mathbf{Q}_l \end{pmatrix} = \begin{bmatrix} \mathbf{A}_{(i,k)} & \mathbf{A}_{(i,l)} \\ \mathbf{A}_{(j,k)} & \mathbf{A}_{(j,l)} \end{bmatrix}. \quad (4)$$

Here, \mathbf{A} represents canonical one-electron or two-electron molecular integrals, e.g., exchange (\mathbf{K}), overlap (\mathbf{S}) or Fock (\mathbf{F}).

The OSV-MP2 correlation energy is computed using $E_c = \langle \mathbf{K}_{(ij,ij)} [2\mathbf{T}_{(ij,ij)} - \mathbf{T}_{(ij,ij)}^\dagger] \rangle$, where the OSV-MP2 amplitudes $\mathbf{T}_{(ij,ij)}$ are approximately decomposed in the third-order many-body expansion, leading to MBE(3)-OSV-MP2 method.⁸ The MBE(3)-OSV-MP2 avoids the full couplings between three or more LMOs, enabling massive parallelization of solving all residual equations. The diagonal amplitudes $\mathbf{T}_{(ii,ii)}$ are obtained in the MBE(3) form,

$$\mathbf{T}_{(ii,ii)} = \mathbf{T}_{(ii,ii)}^i + \sum_k \Delta \mathbf{T}_{(ii,ii)}^{i,k} + \sum_{k>l} \Delta \mathbf{T}_{(ii,ii)}^{i,k,l}, \quad (5)$$

where $\mathbf{T}_{(ii,ii)}^i$ refers to the solution to 1-body clusters, while the 2-body $\Delta\mathbf{T}_{(ii,ii)}^{i,k}$ and 3-body $\Delta\mathbf{T}_{(ii,ii)}^{i,k,l}$ corrections are,

$$\begin{aligned}\Delta\mathbf{T}_{(ii,ii)}^{i,k} &= \mathbf{T}_{(ii,ii)}^{i,k} - \mathbf{T}_{(ii,ii)}^i \\ \Delta\mathbf{T}_{(ii,ii)}^{i,k,l} &= \mathbf{T}_{(ii,ii)}^{i,k,l} - \Delta\mathbf{T}_{(ii,ii)}^{i,k} - \Delta\mathbf{T}_{(ii,ii)}^{i,l} - \mathbf{T}_{(ii,ii)}^i.\end{aligned}\quad (6)$$

Similarly, the off-diagonal pair amplitudes $\mathbf{T}_{(ij,ij)}$ ($i \neq j$) are expanded in MBE(3) as

$$\mathbf{T}_{(ij,ij)} = \mathbf{T}_{(ij,ij)}^{i,j} + \sum_k \Delta\mathbf{T}_{(ij,ij)}^{i,j,k}, \quad (7)$$

with the 3b correction given by

$$\Delta\mathbf{T}_{(ij,ij)}^{i,j,k} = \mathbf{T}_{(ij,ij)}^{i,j,k} - \mathbf{T}_{(ij,ij)}^{i,j}. \quad (8)$$

Above, an n -body (nb) cluster includes n LMOs and their associated OSVs. Each 1b cluster is composed of a single LMO. A 2b cluster combines two 1b clusters, describing correlated LMO pairs ij within the excitation path $(i, j) \rightarrow \bar{\mu}_i \cup \bar{\nu}_j$, that is, a double excitation from ij LMO pairs to their joint OSV subspace $\bar{\mu}_i \cup \bar{\nu}_j$. Similarly, a 3b cluster integrates three 1b clusters, with excitations $(i, j, k) \rightarrow \bar{\mu}_i \cup \bar{\nu}_j \cup \bar{\sigma}_k$. The OSV-MP2 amplitudes $\mathbf{T}_{(ij,ij)}$ explicitly depend on 2b interactions and implicitly on 3b interactions through the second term in eq 2, which can be further simplified by collecting the contributions from MBE clusters without much accuracy loss.

The MBE(3) ansatz further exploits the intrinsic sparsity of explicit third-order contributions to automate selection of only important 2b and 3b interactions, saving substantial computing costs. The sparsity of 2b clusters arises from the shortsightedness of electron correlations, estimated by the average square norm of OSV overlaps before solving MBE(3)-OSV-MP2 equations,

$$s_{ij}^{2b} = \frac{\sum_{\mu\nu} \langle \bar{\mu}_i | \bar{\nu}_j \rangle^2}{\sqrt{n_i^{\text{OSV}} n_j^{\text{OSV}}}}. \quad (9)$$

Extremely distant 2b clusters can be discarded, while weak ones are efficiently recovered via direct

excitation treatment (without exchange blocks) at negligible cost, ensuring linear scaling of strong 2b clusters with system size. The important 3b clusters are determined according to

$$s_{ijk}^{3b} = \frac{1}{3} (s_{ij}^{2b} + s_{ik}^{2b} + s_{jk}^{2b}). \quad (10)$$

Important 3b clusters are identified to give similar accuracy to the original OSV-MP2 calculation. The number of resulting 3b clusters grows linearly. The ability of MBE(3)-OSV-MP2 in independently solving the residual equations for each cluster enhances data locality, eliminates repeated host-device data transfer of intermediates, and significantly lowers inter-process communication and synchronization overheads for updating $\mathbf{T}_{(ij,ij)}$ between parallel tasks. Overall, we see a potentially more efficient GPU-based accelerator to enable massive parallelism on low-scaling MBE(3)-OSV-MP2 than canonical methods.

3 Implementation for Multi-GPU Computing

In data-intensive GPU-based quantum chemistry computations, inefficient non-CUDA operations, such as CPU-bound I/O (e.g., disk or host memory access) and host-device data transfers, often dominate the total runtime. For example, the evaluation of RI-MP2 correlation energy entails $\mathcal{O}(N^5)$ data movement volume, posing significant overheads and poor scalability.^{13,14,56,57} The compact local orbital space of MBE(3)-OSV-MP2 greatly facilitates an optimization of the algorithmic workflow, which further reduces the data transfer cost of MBE(3)-OSV-MP2 calculation to $\mathcal{O}(N^2)$, as detailed below.

Atomic orbital integrals and Fock operator are constructed using CUDA kernels in GPU4PySCF package.^{41,63} In general, NVIDIA’s `cuBLAS` and `cuSolver` libraries provide highly optimized linear algebra routines customized to high-performance operations on large matrices, such as AO-to-MO integral transformations and canonical MP2 calculations. However, for low-rank matrices, such as OSV-based tensors, these libraries do not necessarily outperform custom CUDA kernels. In particular, when handling small matrices, the overhead of repeatedly invoking `cuBLAS`

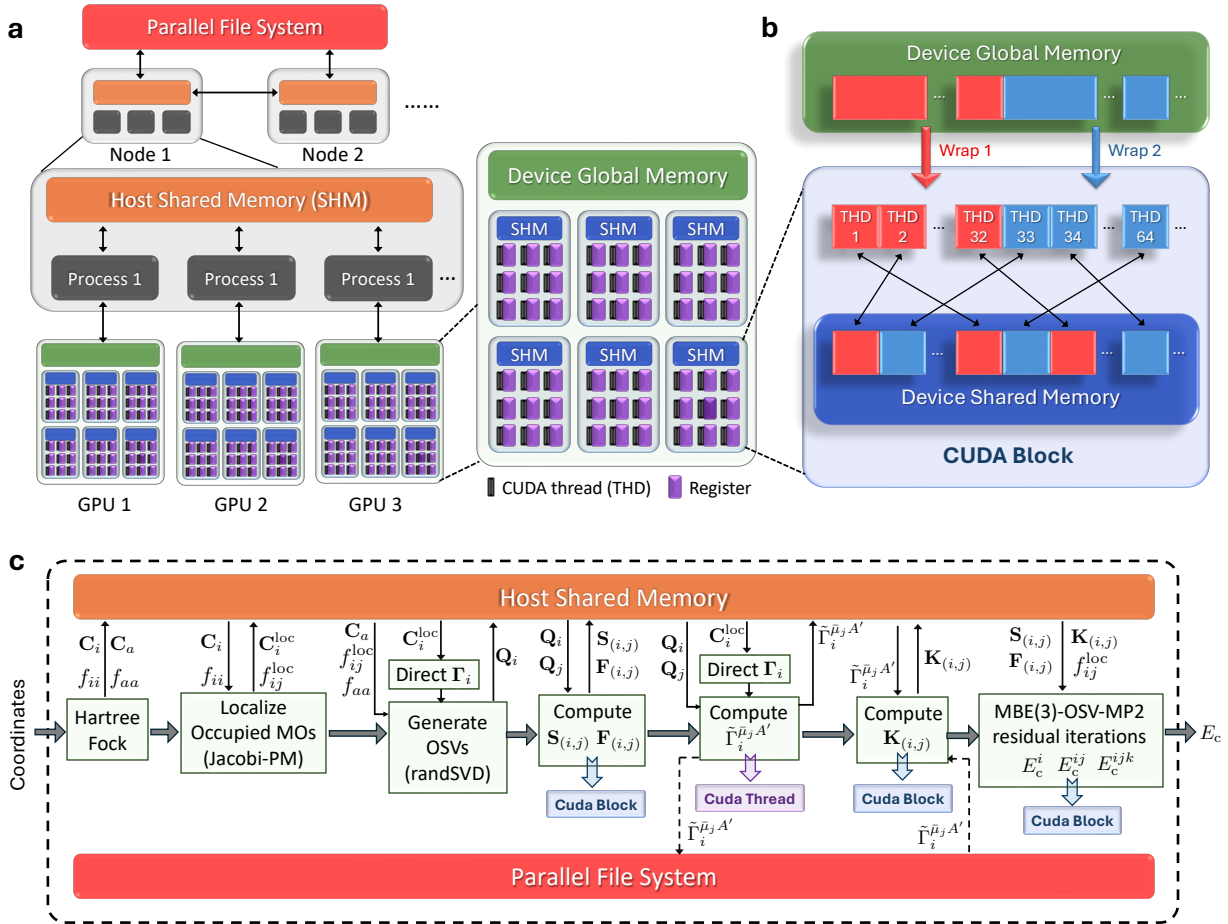


Figure 1: **a.** Multi-GPU parallel architecture. **b.** Coalesced GPU memory access. **c.** GPU parallel scheme for MBE(3)-OSV-MP2.

or `cuSolver` routines can markedly exceed the actual cost of matrix computations. To overcome these limitations, in contrast to many GPU-accelerated canonical MP2 methods that rely on `cuBLAS`, we developed CUDA kernels by mapping LMO pairs or MBE clusters to CUDA thread blocks, explicitly made for MBE(3)-OSV-MP2, to enable efficient parallelization on GPUs and eliminate the excessive overhead launching kernel functions.

The access to GPU global memory is typically limited by low bandwidth and high latency compared to registers and device shared memory. Coalesced access to global memory maximizes effective use of the full bandwidth by allowing warp threads to fetch contiguous addresses in a single transaction, while scattered accesses cause fragmented transactions and latency. As illustrated in Figure 1b, we implemented coalesced offloading mechanisms for OSV-based submatrices

and their efficient reuse via the device shared memory accessible to all threads within the block, substantially enhancing kernel performance while reducing the global memory traffic.

The CPU parallelism is implemented via the Message Passing Interface (MPI), which orchestrates the concurrent execution of multiple GPUs by coordinating tasks distributed across CPU nodes. For better intra-node data communication, the MPI-3 shared memory is utilized to reduce the local memory duplication on all processes and achieves near-zero data exchange latency within the same node. Inter-node data communication is enhanced through passive remote memory access (RMA), which effectively reduces memory copies and synchronization latency, as compared to conventional point-to-point data transmission.

Figure 1c illustrates the MBE(3)-OSV-MP2 computational steps and its parallelization implementation of several bottleneck processes. The GPU calculation begins with Hartree-Fock to determine canonical MO coefficients and energies, followed by the localization of occupied MOs. The density fitting 3-center-2-electron (3c2e) coefficient tensor Γ_i (eq 11) is generated on the fly and then immediately contracted into quantities of much smaller dimension, which avoids huge storage and data movement overheads due to Γ_i size. With Γ_i generator, the randomized SVD is applied to generate and select OSV basis vectors \mathbf{Q}_i according to a single parameter $l_{\text{osv}} = 10^{-4}$. Subsequently, the OSV-based overlap $\mathbf{S}_{(i,j)}$ and Fock $\mathbf{F}_{(i,j)}$ matrices are computed for (i, j) orbital pairs, alongside the calculation of 2b selection metric s_{ij}^{2b} that is tuned by the same parameter l_{osv} . Following this, we compute the OSV-based exchange integrals $\mathbf{K}_{(i,j)}$ in two steps: transforming Γ_i into the OSV-based intermediate $\tilde{\Gamma}_i^{\bar{\mu}_j A'}$, followed by its contraction to $\mathbf{K}_{(i,j)}$. The preconditioning step is then performed for amplitudes updates. Finally, residual equations for MBE clusters are iteratively solved to converge the MP2 correlation energy. Due to compact OSV orbitals and tremendous pair screening, most OSV-based data arrays, including \mathbf{Q}_i , $\mathbf{S}_{(i,j)}$, $\mathbf{F}_{(i,j)}$, $\mathbf{K}_{(i,j)}$ and $\mathbf{T}_{(i,j)}$, are lightweight and thus stored in the host shared memory, which consume, for instance, only a few dozen GB for protein hormone insulin ($\text{C}_{256}\text{H}_{381}\text{N}_{65}\text{O}_{76}\text{S}_6$) with cc-pVTZ basis. The $\tilde{\Gamma}_i^{\bar{\mu}_j A'}$ tensor forms a major storage bottleneck, e.g., ~ 197 GB for insulin/cc-pVTZ, and can be cached in host shared memory when possible or otherwise flushed to disk.

3.1 Direct Density Fitting Integrals

Transformations of two-electron integrals are fundamental and expensive in both Hartree-Fock and MP2 calculations. The utilization of density fitting integrals has been very successful in CPU-based Fock construction, but its application to GPU calculations is disadvantaged by large intermediate 3c2e tensors, creating memory and computation bottlenecks. In contrast, the non-DF Hartree-Fock methods achieve much better GPU parallel efficiency.^{40–42,64}

However, density fitting integrals still substantially reduce MP2 computational costs. Existing GPU-accelerated RI-MP2 implementations either cached the fundamental MO-based 3c2e integrals $(ia|A)$ in memory,^{13,14,56} or on disk.^{53,57} Nevertheless, generating this tensor set requires $\sim 2\times$ its size in temporary storage, for instance, over 17 TB for insulin/cc-pVTZ, imposing severe memory/disk pressure on large systems. Moreover, repeatedly loading $(ia|A)$ and $(jb|A)$ to device memory for each pair incurs massive CPU I/O and host–device transfer overheads. To address these issues, we implemented a direct half-transform integral generator for Γ_i that processes MO batches on the fly (see Algorithm 1). By fully exploiting integral sparsity and permutational symmetry, GPU-based generation of the 3c2e ERIs $(\alpha\beta|A)$ achieves approximately two orders of magnitude higher throughput than the subsequent transformation. Therefore, we regenerate ERIs for each MO batch $\{i\}$, construct Γ_i segments

$$\begin{aligned} (i\alpha|B) &= \sum_{\beta} C_{\beta i}(\beta\alpha|B) \\ \Gamma_i : \Gamma_i^{\alpha A} &= \sum_B (i\alpha|B)V_{AB}^{-1/2}, \end{aligned} \tag{11}$$

and transform them directly to low-rank OSV-based arrays (e.g., $\Gamma_i^{\alpha A} \rightarrow \tilde{\Gamma}_i^{\bar{\mu}j A'}$). This strategy eliminates large intermediate storage and reduces data movement amount to $\mathcal{O}(N^2)$. Moreover, as the localization of occupied orbitals induces sparsity in Γ_i , a compact subset of the LMO-specific

Γ_i is selected when the sum of squared $\Gamma_i^{\alpha A'}$ exceeds a threshold l_{fit} :

$$s_{iA'}^{\text{fit}} = \sum_{\alpha} \left(\Gamma_i^{\alpha A'} \right)^2 > l_{\text{fit}}, A' \in D_i, \quad (12)$$

where only auxiliary orbitals belonging to the domain D_i close to an LMO i are selected.

Algorithm 1 Direct Γ_i generator

- 1: Compute Coulomb kernel 2c2e integrals $V_{AB} = (A|B)$
 - 2: Device memory: Cholesky decomposition of V_{AB} for $V_{AB}^{-1/2}$
 - 3: Transfer MOs \mathbf{C} to device memory
 - 4: **for** MO chunk I in $\{i\}$ on the GPU :
 - 5: Initialize $(I\alpha|B)$ with zeros
 - 6: **for** Sparse AO pair chunk $\beta\alpha$:
 - 7: **for** Fitting orbital chunk $B \in D_I$:
 - 8: Construct $(\beta\alpha|B)$
 - 9: Half-transformation: $(I\alpha|B) += \sum_{\beta} C_{\beta I}(\beta\alpha|B)$
 - 10: Fitting: $\Gamma_I^{\alpha A} = \sum_{B \in D_I} (I\alpha|B) V_{AB}^{-1/2}$
 - 11: Perform OSV generation or $\tilde{\Gamma}_I^{\mu_j A'}$ computation.
-

3.2 Occupied Orbital Localization

We implemented PM localization algorithm using Jacobi sweeps⁶² and Löwdin charges on GPUs, a stable and efficient pairwise-rotation method widely adopted in quantum chemistry programs.⁶⁵⁻⁶⁷

As shown in Algorithm 2, the Löwdin charge tensor P_{ij}^A is initialized for an atom A based on the symmetrically orthonormalized and PM localized MOs $\tilde{\mathbf{C}} = \mathbf{S}^{1/2}\mathbf{C}\mathbf{U}$ using a custom CUDA kernel on GPUs. The resulting local MOs maximize the PM charges on each atom,

$$L = \sum_{iA} (P_{ii}^A)^2. \quad (13)$$

For each (i, j) pair with $i < j$, the rotation angle θ can be determined with CUDA kernels using

$$a_{ij} = \sum_A (P_{ij}^A)^2 - \frac{1}{4} (P_{ii}^A - P_{jj}^A)^2, \quad b_{ij} = \sum_A P_{ij}^A (P_{ii}^A - P_{jj}^A), \quad \theta = \frac{1}{4} \arctan \left(\frac{b_{ij}}{-a_{ij}} \right). \quad (14)$$

The orbital rotation U_{ij} can be computed in parallel by distributing k rows on CUDA threads, which updates P_{ij}^A pair-wisely for each ij at a time,

$$(P_{ki}^A)^{\text{new}} = P_{ki}^A \cos\theta + P_{kj}^A \sin\theta, \quad (P_{kj}^A)^{\text{new}} = P_{kj}^A \cos\theta - P_{ki}^A \sin\theta. \quad (15)$$

The localization procedure completes when the incremental functional falls below a localization threshold

$$\Delta L = \sum_{ij} \sqrt{a_{ij}^2 + b_{ij}^2} (1 - \cos 4\theta) < l_{\text{loc}}, \quad (16)$$

where typically $l_{\text{loc}} = 10^{-3}$.

Algorithm 2 Occupied orbital localization with Jacobi sweeps

- 1: Initialize identity matrix U_{ij} on GPU
 - 2: Initialize canonical $P_{ij}^A = \sum_{\alpha \in \mathcal{A}} \tilde{C}_{\alpha i} \tilde{C}_{\alpha j}$ on GPU
 - 3: **while** $\Delta L > l_{\text{loc}}$:
 - 4: $\Delta L = 0.0$
 - 5: **for** (i, j) pair if $i < j$:
 - 6: Compute a_{ij} , b_{ij} and θ using equations in eq 14
 - 7: **if** $|\sin\theta| \geq 10^{-10}$:
 - 8: $\Delta L += \sqrt{a_{ij}^2 + b_{ij}^2} (1 - \cos 4\theta)$
 - 9: Rotate columns U_{ki} and U_{kj}
 - 10: Rotate first MO index P_{ik}^A and P_{jk}^A
 - 11: Rotate second MO index P_{ki}^A and P_{kj}^A
 - 12: Transfer U_{ij} to host memory
-

3.3 Randomized OSV generation

The diagonalization of the semi-canonical MP2 diagonal amplitudes for generating OSVs in eq 3 has a formal scaling of $\mathcal{O}(N^4)$ over all LMOs, posing a bottleneck for computing macromolecules. We previously reduced this scaling to $\mathcal{O}(N^2)$ via interpolative decomposition (ID). However, the cost of ID-OSV generation increases rapidly by expanding the column subset of \mathbf{T}_{ii} matrix as needed for better accuracy. Alternatively, random projections effectively approximate the dominant

row subspace of \mathbf{T}_{ii} ,⁶⁸

$$\mathbf{Y} = \mathbf{G}\mathbf{T}_{ii}, \quad (17)$$

where \mathbf{G} is $N_{\text{rosv}} \times N_{\text{vir}}$ random Gaussian matrix, with N_{vir} denoting the number of canonical virtual orbitals and N_{rosv} the number of the sampled rows of \mathbf{Y} . Typically, there is $N_{\text{rosv}} \ll N_{\text{vir}}$ due to the rapid decay of \mathbf{T}_{ii} singular values, which ensures a rather low OSV generation cost that grows only linearly with N_{vir} . In our implementation, the N_{rosv} rows of \mathbf{Y} are incrementally sampled by fulfilling the following condition for every $r = 10$ rows,

$$\max \{ \|\mathbf{y}^{(s+1)}\|, \|\mathbf{y}^{(s+2)}\|, \dots, \|\mathbf{y}^{(s+r)}\| \} \leq l_{\text{osv}} / (10\sqrt{2/\pi}). \quad (18)$$

Subsequently, the selected rows are orthonormalized in eq 19 to transform the amplitude in eq 20.

$$\mathbf{Z} = \text{orth}(\mathbf{Y}) \quad (19)$$

$$\tilde{\mathbf{T}}_{ii} = \mathbf{Z}\mathbf{T}_{ii} \quad (20)$$

The transformed amplitude is further decomposed via singular value decomposition in eq 21, followed by a back-transformation to obtain the OSV basis vector \mathbf{Q}_i in eq 22.

$$\tilde{\mathbf{T}}_{ii} = \tilde{\mathbf{Q}}_i \omega_i \tilde{\mathbf{V}}_i^\dagger, \quad (21)$$

$$\mathbf{Q}_i = \mathbf{Z}^\dagger \tilde{\mathbf{Q}}_i. \quad (22)$$

The randomized OSV (rOSV) generator is implemented as Algorithm 3. The calculation of the semi-canonical diagonal MP2 amplitudes is substantially expedited through the sparse fitting of eq 12,

$$\tilde{\Gamma}_i^{aA'} = \sum_{\alpha} C_{\alpha a} \Gamma_i^{\alpha A'}, A' \in D_i, \quad T_{ii}^{ab} = \sum_{A' \in D_i} \frac{\tilde{\Gamma}_i^{aA'} \tilde{\Gamma}_i^{bA'}}{f_{aa} + f_{bb} - 2f_{ii}}. \quad (23)$$

The low-rank randomized projection matrix \mathbf{Z} (defined in eq 19) is built incrementally using the adaptive randomized range finder.⁶⁸ A row-based implementation is employed to improve memory

Algorithm 3 Randomized OSV generation

- 1: Transfer $f_{aa}, C_{\beta a}, C_{\beta i}$ and $V_{PQ}^{-1/2}$ to device memory
 - 2: **for** chunk I in $\{i\}$ on the GPU :
 - 3: Generate $(I\alpha|B)$ using Algorithm 1
 - 4: **for** i in chunk I :
 - 5: Compute $\Gamma_i^{\alpha A'} = \sum_B (i\alpha|B) V_{BA'}^{-1/2}, A' \in \{A'\}_i$
 - 6: Compute T_{ii}^{ab} from $\Gamma_i^{\alpha A'}$ using eq 23.

 - 7: ““ Adaptive randomized range finder ””
 - 8: Initialize selected rows $s = 0$
 - 9: Generate $\mathbf{Y} = \mathbf{G}\mathbf{T}_{ii}$, where \mathbf{G} is an $N_{\text{rosv}} \times N_{\text{vir}}$ standard Gaussian matrix
 - 10: Generate $\bar{\mathbf{Y}} = \bar{\mathbf{G}}\mathbf{T}_{ii}$, where $\bar{\mathbf{G}}$ is an $N_{\text{rosv}}^{\text{max}} \times N_{\text{vir}}$ standard Gaussian matrix
 - 11: Pre-allocate $N_{\text{rosv}}^{\text{max}} \times N_{\text{vir}}$ array to initialize $\mathbf{Z}^{(0)} = []$
 - 12: **while** $\max \{ \|\mathbf{y}^{(s+1)}\|, \|\mathbf{y}^{(s+2)}\|, \dots, \|\mathbf{y}^{(s+r)}\| \} > l_{\text{osv}} / (10\sqrt{2/\pi}) :$
 - 13: $s += 1$
 - 14: Compute $\mathbf{z}^{(s)}$ orthonormal to $\mathbf{Z}^{(s-1)}$ from $\mathbf{y}^{(s)}$ using eq 24
 - 15: Appending: $\mathbf{Z}^{(s)} = \begin{bmatrix} \mathbf{Z}^{(s-1)} \\ \mathbf{z}^{(s)} \end{bmatrix}$
 - 16: Shift block $\mathbf{y}^{(t)} \leftarrow \mathbf{y}^{(t+1)}, t = s, \dots, s+r-1$
 - 17: Compute $\mathbf{y}^{(s+r)} = \bar{\mathbf{y}}^{(s)} [\mathbf{I} - (\mathbf{Z}^{(s-1)})^\dagger \mathbf{Z}^{(s-1)}]$
 - 18: Compute $\mathbf{Y} -= \mathbf{Y} (\mathbf{z}^{(s)})^\dagger \mathbf{z}^{(s)}$
 - 19: Compute $\tilde{\mathbf{T}}_{ii} = \mathbf{Z}\mathbf{T}_{ii}$
 - 20: Low-rank SVD: $\tilde{\mathbf{T}}_{ii} = \tilde{\mathbf{Q}}_i \omega_i \tilde{\mathbf{V}}_i^\dagger$
 - 21: Compute OSV matrix: $\mathbf{Q}_i = \mathbf{Z}^\dagger \tilde{\mathbf{Q}}_i$.
 - 22: Select \mathbf{Q}_i vectors with $\omega_i \geq l_{\text{osv}}$
 - 23: Transfer \mathbf{Q}_i to host shared memory
-

efficiency. The range finder uses Gram-Schmidt orthogonalization to ensure the new row $\mathbf{z}^{(s)}$ is orthonormal to all prior rows $\mathbf{Z}^{(s-1)}$:

$$\tilde{\mathbf{z}}^{(s)} = \mathbf{y}^{(s)} \left[\mathbf{I} - (\mathbf{Z}^{(s-1)})^\dagger \mathbf{Z}^{(s-1)} \right], \quad \mathbf{z}^{(s)} = \tilde{\mathbf{z}}^{(s)} / \|\tilde{\mathbf{z}}^{(s)}\|, \quad (24)$$

where $\mathbf{y}^{(s)} = \mathbf{g}^{(s)} \mathbf{T}_{ii}$ and $\mathbf{g}^{(s)}$ is a $1 \times N_{\text{vir}}$ Gaussian random vector at the row s . The $r \times N_{\text{vir}}$ matrix \mathbf{Y} is iteratively accumulated. To reduce computational latency from frequent small-matrix multiplications and random vector generation, the new rows $\mathbf{g}^{(s+r)} \mathbf{T}_{ii}$ are precomputed. The rOSV rank N_{rOSV} is oversampled for enhancing accuracy, and the resulting \mathbf{Q}_i in eq 22 can be further pruned by removing columns corresponding to eigenvalues $\omega_i < l_{\text{osv}}$. In this compact OSV representation, the \mathbf{Q}_i vectors are small enough (~ 9 GB for insulin/cc-pVTZ) to be stored in host shared memory and can be efficiently fetched with near-zero-latency in the following pairwise calculations.

3.4 OSV Overlap and Fock Computation

In our previous CPU-based implementation for computing OSV overlap $\mathbf{S}_{(i,j)}$ and Fock $\mathbf{F}_{(i,j)}$ matrices,⁸ \mathbf{Q}_i and \mathbf{Q}_j are loaded for every (i,j) pair in parallel via remote memory access, which is problematic to GPUs due to an excessive data transfer volume as $(N_{\text{occ}} + 1)N_{\text{occ}}N_{\text{vir}}N_{\text{osv}}$ from the host to the device. To address this, we revamp the data transfer mechanism from a pair-wise to an LMO-wise implementation, by batching LMOs out of all pairs, and the batch length is determined by available device global memory. The number of batches is minimized by greedily selecting sorted pairs that group no more than N_i^{batch} unique LMOs, as detailed in Algorithm 4. All \mathbf{Q}_i vectors specific to LMOs belonging to each batch are transferred to device global memory. The computations of pair $\mathbf{S}_{(i,j)}$ and $\mathbf{F}_{(i,j)}$ are mapped to CUDA blocks for extensive parallelization. To enable coalesced access, f_{aa} and \mathbf{Q}_i are further loaded to device shared memory along virtual orbital slices according to the pre-allocated shared memory per CUDA block. After computing $\mathbf{S}_{(i,j)}$ and $\mathbf{F}_{(i,j)}$, the 2b cluster criteria s_{ij}^{2b} are evaluated by performing parallel reduction from threads within the block. Based on the 2b and 3b selection metrics defined in eqs 9 and 10,

2b clusters are classified into 3 categories for different treatments: distant ($s_{ij}^{2b} < 10^{-7}$), weak ($10^{-7} \leq s_{ij}^{2b} < 10^{-2}$) and close ($s_{ij}^{2b} \geq 10^{-2}$). Unimportant 3b clusters with $s_{ijk}^{3b} < 0.2$ are discarded. Only the $\mathbf{S}_{(i,j)}$ and $\mathbf{F}_{(i,j)}$ for non-distant pairs are stored in the host shared memory.

Algorithm 4 Minimal Batches of LMOs for Pairs

- 1: **Inputs:** pairs, N_i^{batch}
 - 2: Extract all unique LMOs from pairs
 - 3: **for** LMO i :
 - 4: Count the total number of occurrences of i among all pairs (n_i)
 - 5: Sort pairs in the descending order of $n_i + n_j$ for each ij pair
 - 6: Generate LMO batches among all sorted pairs: each batch contains pairs that possess at most N_i^{batch} LMOs
 - 7: **Outputs:** batches of LMOs and pairs
-

Algorithm 5 $\mathbf{S}_{(i,j)}$ and $\mathbf{F}_{(i,j)}$ Computation

- 1: Transfer f_{aa} to device global memory
 - 2: Generate LMO batches using Algorithm 4
 - 3: **for** batch LMOs K :
 - 4: Transfer all \mathbf{Q}_K vectors to device global memory
 - 5: Map pairs to CUDA blocks belonging to batch K
 - 6: **In** CUDA block with pair (i, j) :
 - 7: Batch virtual orbitals to fit device shared memory
 - 8: **for** chunk a in full virtual $\{a\}$:
 - 9: Coalesced load of f_{aa} , $Q_i^{a\bar{\mu}_i}$ and $Q_j^{a\bar{\nu}_j}$ to device shared memory
 - 10: Compute $S_{ij}^{\bar{\mu}_i\bar{\nu}_j} += \sum_a Q_i^{a\bar{\mu}_i} Q_j^{a\bar{\nu}_j}$
 - 11: Compute $F_{ij}^{\bar{\mu}_i\bar{\nu}_j} += \sum_a Q_i^{a\bar{\mu}_i} f_{aa} Q_j^{a\bar{\nu}_j}$
 - 12: Parallel reduction: $s_{ij}^{2b} = \sum_{\mu\nu} \left(S_{ij}^{\bar{\mu}_i\bar{\nu}_j} \right)^2 / \sqrt{n_i n_j}$
 - 13: Transfer $\mathbf{S}_{(i,j)}$, $\mathbf{F}_{(i,j)}$ and s_{ij}^{2b} back to host memory
 - 14: Perform pair classification based on s_{ij}^{2b}
 - 15: Store $\mathbf{S}_{(i,j)}$ and $\mathbf{F}_{(i,j)}$ in host shared memory for kept pairs
-

3.5 OSV Exchange Integrals

The OSV exchange integrals $\mathbf{K}_{(ij,ij)}$ are formulated in eq 4 where the AO-to-OSV transformation matrices \mathbf{Q}_i are cached in host shared memory. Due to the compact OSV space, we can avoid loading large $\mathbf{\Gamma}_i$ and $\mathbf{\Gamma}_j$ for every LMO pair that is a common implementation for RI-MP2 GPU

Algorithm 6 OSV Exchange Integral Evaluation

- 1: ““ $\tilde{\Gamma}_i^{\tilde{\mu}_j A'}$ evaluation ””
 - 2: Sort process LMOs $\{i\}$ and their close $\{j\}$
 - 3: Transfer first batch of \mathbf{Q}_j to device global memory
 - 4: **for** LMO chunk I on the GPU :
 - 5: Generate Γ_I using Algorithm 1
 - 6: **for** i in chunk I :
 - 7: Update \mathbf{Q}_j for j close to i
 - 8: Map $\tilde{\Gamma}_i^{\tilde{\mu}_j A'}$ elements to CUDA threads
 - 9: **In** each CUDA block:
 - 10: Batch atomic orbitals by shared memory availability
 - 11: Fetch $\Gamma_i^{\alpha A'}$ and $Q_j^{\alpha \tilde{\mu}_j}$ to device shared memory for the first AO batch
 - 12: **for** chunk α in $\{\alpha\}$:
 - 13: Fetch $\Gamma_i^{\alpha A'}$ and $Q_j^{\alpha \tilde{\mu}_j}$ for the next AO batch
 - 14: Compute $\tilde{\Gamma}_i^{\tilde{\mu}_j A'} += \sum_{\alpha} Q_j^{\alpha \tilde{\mu}_j} \Gamma_i^{\alpha A'}$
 - 15: Write $\tilde{\Gamma}_i^{\tilde{\mu}_j A'}$ to global memory
 - 16: Store $\tilde{\Gamma}_i^{\tilde{\mu}_j A'}$ in host shared memory or on disk

 - 17: ““ $\tilde{\Gamma}_i^{\tilde{\mu}_j A'}$ contraction ””
 - 18: Generate LMO batches using Algorithm 4
 - 19: **for** batch LMOs K :
 - 20: Transfer diagonal pair $\tilde{\Gamma}_K^{\tilde{\mu}_K A'}$ to device global memory
 - 21: Make close pair batches to fit device global memory
 - 22: **for** batch close pairs (i, j) :
 - 23: Transfer $\tilde{\Gamma}_i^{\tilde{\mu}_j A'}$ and $\tilde{\Gamma}_j^{\tilde{\mu}_i A'}$ to device global memory
 - 24: **In** CUDA block with close pair (i, j) :
 - 25: Batch fitting AOs to fit device shared memory
 - 26: **for** chunk A' in $\{A'\}_i \cup \{A'\}_j$:
 - 27: Fetch $\tilde{\Gamma}_i^{\tilde{\mu}_i A'}$, $\tilde{\Gamma}_j^{\tilde{\mu}_j A'}$, $\tilde{\Gamma}_i^{\tilde{\mu}_j A'}$ and $\tilde{\Gamma}_j^{\tilde{\mu}_i A'}$ to device shared memory
 - 28: Compute $\mathbf{K}_{(ij,ij)}$ using eq 26
 - 29: **for** batch weak pairs (i, j) :
 - 30: **In** CUDA block with weak pair (i, j) :
 - 31: Batch fitting AOs to fit device shared memory
 - 32: **for** chunk A' in $\{A'\}_i \cup \{A'\}_j$:
 - 33: Fetch $\tilde{\Gamma}_i^{\tilde{\mu}_i A'}$ and $\tilde{\Gamma}_j^{\tilde{\mu}_j A'}$ to device shared memory
 - 34: Compute $\mathbf{K}_{(i,j)}$ using eq (27)
 - 35: Transfer $\mathbf{K}_{(ij,ij)}$ and $\mathbf{K}_{(ij)}$ to host shared memory
-

algorithms.^{13,14,56,57,69,70} Here we adopt a two-step workflow by first computing the OSV-based half-transformed integrals as

$$\tilde{\Gamma}_i^{\bar{\mu}_j A'} = \sum_{\alpha} Q_j^{\alpha \bar{\mu}_j} \Gamma_i^{\alpha A'}, A' \in D_i \cup D_j \quad (25)$$

where the sparse fitting basis A' belongs to the union of the domains D_i and D_j . Γ_i in eq 25 is generated on the fly, eliminating storage and I/O overhead. Small Q_j tensors can be reused across several LMOs to avoid excessive data transmissions. The OSV-based $\tilde{\Gamma}_i$ is substantially reduced compared to Γ_i , which therefore can be stored in memory or on disk. The second step makes rapid contraction of $\tilde{\Gamma}_i^{\bar{\mu}_j A'}$ for close and weak 2b clusters in eqs 26 and 27, respectively.

$$\begin{pmatrix} K_{ij}^{\bar{\mu}_i \bar{\mu}_i} & K_{ij}^{\bar{\mu}_i \bar{\nu}_j} \\ K_{ij}^{\bar{\nu}_j \bar{\mu}_i} & K_{ij}^{\bar{\nu}_j \bar{\nu}_j} \end{pmatrix} = \sum_{A'} \begin{bmatrix} \tilde{\Gamma}_i^{\bar{\mu}_i A'} \\ \tilde{\Gamma}_i^{\bar{\nu}_j A'} \end{bmatrix} \begin{bmatrix} \tilde{\Gamma}_j^{\bar{\mu}_i A'} & \tilde{\Gamma}_i^{\bar{\nu}_j A'} \end{bmatrix}, A' \in D_i \cup D_j, \quad (26)$$

$$K_{ij}^{\bar{\mu}_i \bar{\nu}_j} = \sum_{A'} \tilde{\Gamma}_i^{\bar{\mu}_i A'} \tilde{\Gamma}_j^{\bar{\nu}_j A'}, A' \in D_i \cup D_j. \quad (27)$$

Custom CUDA kernels are implemented for eqs 25-27 in Algorithm 6, which slices Γ_i and Q_j into AO batches to fit the device shared memory and bandwidth consumption. In addition, the double buffering is used to overlap processes of data fetching and computation during the construction of $\tilde{\Gamma}_i$, with each element assigned to a CUDA thread and accumulated in registers. The $\tilde{\Gamma}_i$ contractions in eqs 26 and 27 are mapped pair-wisely to CUDA blocks, which are placed in device shared memory to reduce otherwise repeated access to global memory.

3.6 MBE(3)-OSV-MP2 Residual Equations

Our GPU implementation for solving residual equations is described in Algorithm 7. All intermediates in OSV basis corresponding to unique LMO pairs are loaded into the device global memory only for each batch of MBE clusters, which naturally reduces both memory usage and data transfer. An individual residual equation for a given cluster is solved independently on each CUDA

Algorithm 7 Residual Iterations

- 1: ““ For close MBE clusters ””
 - 2: **for** batch MBE cluster :
 - 3: Get unique LMO pairs from the batch clusters
 - 4: Transfer f_{ij} , $\mathbf{S}_{(i,j)}$, $\mathbf{F}_{(i,j)}$, $\mathbf{K}_{(ij,ij)}$, $\mathbf{X}_{(ij,ij)}$, $\tilde{\mathbf{E}}_{(ij,ij)}$ and $\mathbf{T}_{(i,j)}$ to device global memory
 - 5: Map MBE clusters to CUDA blocks
 - 6: **In** CUDA block with MBE cluster:
 - 7: Initialize E_c^{current} , E_c^{last} and $\mathbf{T}_{(ij,ij)}$
 - 8: **while** $(E_c^{\text{current}} - E_c^{\text{last}}) \geq l_{\text{mp2e}}$:
 - 9: $E_c^{\text{last}} = E_c^{\text{current}}$
 - 10: $E_c^{\text{current}} = 0.0$
 - 11: **for** pair (i, j) from cluster :
 - 12: Compute $\mathbf{R}_{(ij,ij)}$ using eq (2)
 - 13: Transform $\tilde{\mathbf{R}}_{(ij,ij)} = \mathbf{X}_{(ij,ij)}^\dagger \mathbf{R}_{(ij,ij)} \mathbf{X}_{(ij,ij)}$
 - 14: Update $\mathbf{T}_{(ij,ij)} += \mathbf{X}_{(ij,ij)} (\tilde{\mathbf{R}}_{(ij,ij)} / \tilde{\mathbf{E}}_{(ij,ij)}) \mathbf{X}_{(ij,ij)}^\dagger$
 - 15: $E_c^{\text{current}} += \langle \mathbf{K}_{(ij,ij)} (2\mathbf{T}_{(ij,ij)} - \mathbf{T}_{(ij,ij)}^\dagger) \rangle$
 - 16:
 - 17: Accumulate cluster $\mathbf{T}_{(ij,ij)}$ to host shared memory
 - 18: Accumulate E_c^{current} to total E_c
 - 19: ““ For weak pairs ””
 - 20: Generate LMO batches using Algorithm 4
 - 21: **for** batch k :
 - 22: Transfer $\mathbf{T}_{(k,k)}$, $\mathbf{X}_{(k,k)}$ and $\tilde{\mathbf{E}}_{(k,k)}$ to device global memory
 - 23: Transfer f_{ij} , $\mathbf{S}_{(i,j)}$, $\mathbf{F}_{(i,j)}$ and $\mathbf{K}_{(i,j)}$ to device global memory
 - 24: Map weak pairs formed by k to CUDA blocks
 - 25: **In** CUDA block with weak pair (i, j) :
 - 26: Compute $\mathbf{R}_{(i,j)}$ using eq (28)
 - 27: Transform $\tilde{\mathbf{R}}_{(i,j)} = \mathbf{X}_{(i,i)}^\dagger \mathbf{R}_{(i,j)} \mathbf{X}_{(j,j)}$
 - 28: Compute $\mathbf{T}_{(i,j)} = \mathbf{X}_{(i,i)} \left[\tilde{\mathbf{R}}_{(i,j)} / (f_{ii} + f_{jj} - \tilde{\mathbf{E}}_{(i,i)} - \tilde{\mathbf{E}}_{(j,j)}) \right] \mathbf{X}_{(j,j)}^\dagger$
 - 29: Compute $E_c^{ij} = 2 \langle \mathbf{K}_{(i,j)} \mathbf{T}_{(i,j)} \rangle$
 - 30: Accumulate E_c^{ij} to total E_c
-

block. Evaluating the 4-block residual matrix $\mathbf{R}_{(ij,ij)}$ involves the composite matrix $\mathbf{S}_{(ij,kl)}$ and $\mathbf{F}_{(ij,kl)}$, whose sub-blocks are scattered across non-contiguous memory regions. To avoid conditional branching and thread divergence in a unified loop, each sub-block of $\mathbf{R}_{(ij,ij)}$ is computed separately.

Among the tremendous amount of weak pairs, the exchange excitations ($i \rightarrow \bar{\mu}_j, j \rightarrow \bar{\nu}_i$) are negligible for such long-range interactions. Therefore single-block residual equations $\mathbf{R}_{(i,j)}$, which are a drastic simplification of the full residual equations $\mathbf{R}_{(ij,ij)}$, are sufficiently accurate,

$$\mathbf{R}_{(i,j)} = \mathbf{K}_{(i,j)} + \mathbf{T}_{(i,j)}\mathbf{F}_{(j,i)} + \mathbf{F}_{(i,i)}\mathbf{T}_{(i,j)} - (f_{ij} + f_{ii})\mathbf{T}_{(i,j)} - f_{ij} [\mathbf{T}_{(i,i)}\mathbf{S}_{(i,j)} + \mathbf{S}_{(i,i)}\mathbf{T}_{(j,j)}]. \quad (28)$$

Since weak-pair amplitudes $\mathbf{T}_{(i,j)}$ couple exclusively to the pre-computed diagonal-pair amplitudes, they can be determined directly without iteration. This feature along with the one-block residual formulation makes the evaluation cost negligible for long-range correlation energies, as compared to that of solving close pair residual equations.

The update of $\mathbf{T}_{(ij,ij)}$ amplitudes constitutes another computational bottleneck in solving close pair residual equations, as the generalized eigenvalue problem is targeted for each close pair (i, j) ,

$$\mathbf{F}_{(ij,ij)}\mathbf{X}_{(ij,ij)} = \mathbf{S}_{(ij,ij)}\mathbf{X}_{(ij,ij)}\tilde{\mathbf{E}}_{(i,j)}, \quad (29)$$

where $\mathbf{X}_{(ij,ij)}$ and $\tilde{\mathbf{E}}_{(i,j)}$ denote the eigenvectors and eigenvalues, respectively. On CPUs, this equation can be conveniently solved for each pair assigned to an MPI process via Cholesky decomposition. GPU implementations, however, suffer from significant overhead: the repeated invocation of `cuSolver`'s eigenvalue solver is much more expensive than the computation itself, due to the small size of OSV-based matrices. We eliminate this overhead by constructing a CUDA kernel to enable pair-wise diagonalizations over blocks. Furthermore, in the CUDA kernel, we implement a device function to carry out block-wise Cholesky factorization $\mathbf{S}_{(ij,ij)} = \mathbf{L}_{(ij)}\mathbf{L}_{(ij)}^\dagger$, where the elements of the lower-triangular factor $\mathbf{L}_{(ij)}$ are determined in parallel across successive column iterations. A Jacobi diagonalization routine is adapted for small OSV-based matrices, where

all eigenvalue updates and eigenvector rotations are executed concurrently on threads within each block similar to Algorithm 2. We develop another device function that solves triangular eigen-systems involving $\mathbf{L}_{(ij)}$, thereby avoiding explicit computation of the numerically unstable inverse $\mathbf{L}_{(ij)}^{-1}$. The pre-allocated device shared memory in each thread block is reserved across device functions to cache intermediate quantities and accumulate partial results, significantly reducing global memory accesses and enhancing overall computational performance.

4 Results

In all MBE(3)-OSV-MP2 calculations presented in this work, we adopt the truncation thresholds for determining various local orbital spaces that were previously optimized for an optimal efficiency–accuracy trade-off.⁸ The sparsity identified by these cutoff thresholds is demonstrated with insulin/cc-pVTZ in Table 1. Numerical benchmarks demonstrate that the correlation energy accuracy from our GPU-accelerated MBE(3)-OSV-MP2 implementation is comparable to the previously reported CPU-based results, as shown in Table S1.

To assess the computational performance and scalability of the GPU acceleration, we evaluate the capability of our implementation for efficiently handling large molecules and provide timing comparisons with other GPU-accelerated RI-MP2 implementations^{13,57} as well as our own CPU-based algorithm.⁸ All computations in this study were performed on the Tianhe-2 supercomputer at the National Supercomputing Center. Our GPU computations utilized 1–3 nodes, each equipped with $8 \times$ NVIDIA A800 (80 GB) GPUs connected via PCIe 4.0 $\times 16$, along with Lustre parallel file system. CPU calculations employed 64 cores on Intel Xeon Platinum 8360Y (2.60 GHz).

Table 1: The chosen cutoff parameters for predefining orbital and MBE cluster spaces in MBE(3)-OSV-MP2 calculations and the resulting sparsity (demonstrated with insulin/cc-pVTZ).

	Threshold	Full	Kept	Sparsity (%)
AO pairs	10^{-10}	304432704	25267990	91.70
Average MP2 sparse fitting	10^{-6}	44319	5957	86.56
Average OSVs	10^{-4}	15910	70	99.56
Close 2-body clusters	10^{-2}	617716	21204	96.57
3-body clusters	0.2	227938315	59456	99.97

4.1 GPU Parallel Scalability with Molecular Sizes

Figure 2 compares the wall time and scaling performance of individual MBE(3)-OSV-MP2 steps on a single NVIDIA A800 (80 GB) GPU. The MBE(3)-OSV-MP2 energy calculation was completed within about 400 s for the longest polymer (Gly)₄₀ on 5723 atomic basis functions. Overall, the GPU MBE(3)-OSV-MP2 energy calculation scales much more favorably by $\mathcal{O}(N^{1.9})$ than our previous CPU implementation,⁸ demonstrating better task parallel efficiency for large-scale simulations. The GPU calculation is dominated by the on the fly construction of Γ_i for which both the scaling complexity of $\mathcal{O}(N^{2.6})$ and timing fraction are relatively high compared to other steps. Excluding the orbital localization and Γ_i build, all of other MBE(3)-OSV-MP2 computational steps scale only as $\mathcal{O}(N^{1.3})$, due to both parallel algorithm improvements and chip advancements, compared to the $\mathcal{O}(N^{2.1})$ scaling of the CPU computation.⁸

Several other CPU computational bottlenecks are now alleviated because of their algorithmic adaptation to GPU device. The orbital localization on GPU becomes only a minor fraction of the total computational cost with an empirical scaling $\mathcal{O}(N^{2.1})$, which is much reduced from the formal $\mathcal{O}(N^3)$ complexity. The GPU-based rOSV generation scales only as $\mathcal{O}(N^{1.5})$, making a substantial improvement over the ID-OSV scaling of $\mathcal{O}(N^{2.5})$.⁸ The sparsity exploration in LMO pairs, OSVs and auxiliary fitting space considerably accelerates the GPU evaluations of OSV overlap, Fock and exchange tensors, which add up to only a small portion of the total runtime. Finally, both the preconditioning and residual iterations exhibit a linear scaling, managed by effective truncations

of OSVs and MBE 2b/3b clusters.

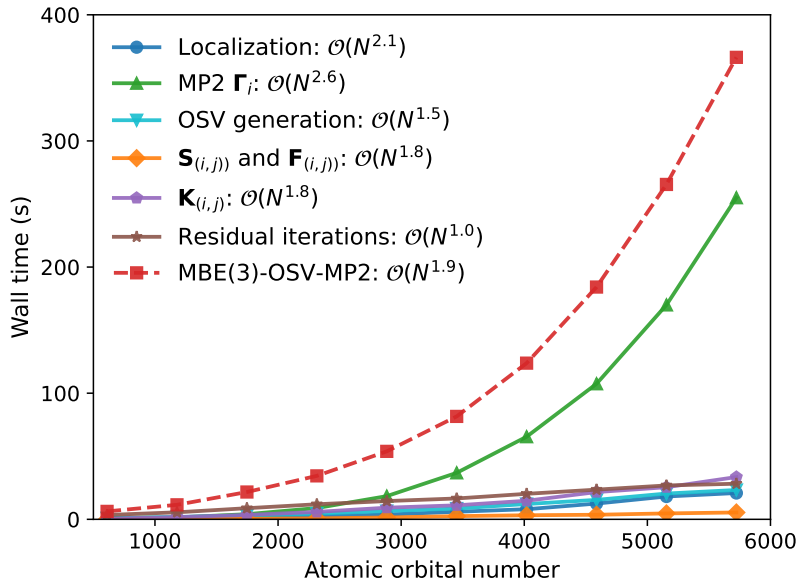


Figure 2: The comparison of the total Wall time (seconds) as a function of the number of atomic orbitals for MBE(3)-OSV-MP2 and its individual computing components using one NVIDIA A800 (80 GB) GPU. All timings of polyglycines $(\text{Gly})_n$ ($n = 4, 8, \dots, 40$) were obtained using def2-TZVP/def2-TZVP-RIFit basis sets.

4.2 Speedup Scalability with GPU numbers

The GPU parallel speedup performance of MBE(3)-OSV-MP2 computation is demonstrated up to 24 A800 (80 GB) GPUs across 3 nodes for $(\text{H}_2\text{O})_{100}$ and $(\text{H}_2\text{O})_{300}$ which are optimized with ChargeNN model,⁷¹ as shown in Figure 3. The localization is excluded from MBE(3)-OSV-MP2 parallel tests as it was performed on only one GPU and the multi-GPU localization has not been implemented. The MBE(3)-OSV-MP2 calculation shows scalable acceleration for the large $(\text{H}_2\text{O})_{300}$ cluster with the number of GPU. The parallel efficiency is still maintained by $\sim 90\%$ up to 16 GPUs and only moderately drops to 84% on 24 GPUs. For the smaller $(\text{H}_2\text{O})_{100}$ cluster, however, the efficiency descends markedly to 47% on 16 GPUs and 34% on 24 GPUs, because the relatively low computational intensity per task for small systems is insufficient to effectively mask non-kernel overheads, such as communication, synchronization, and host–device transfers.

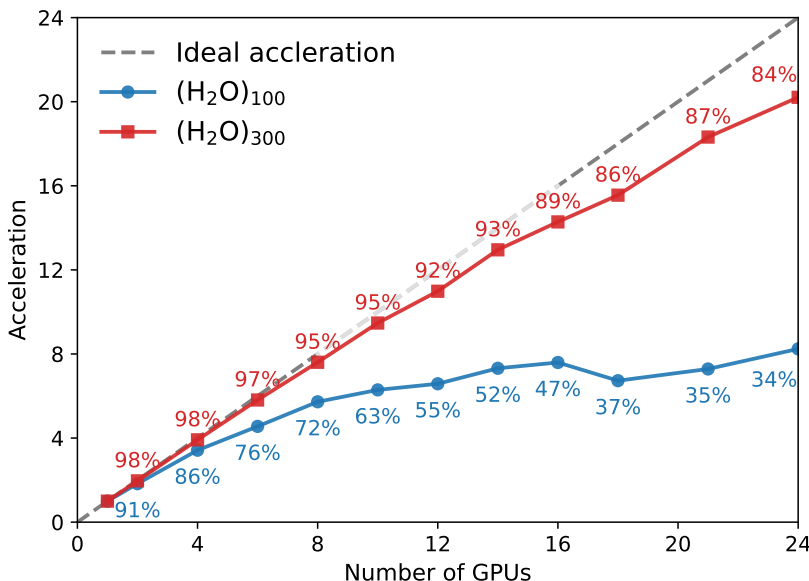


Figure 3: Strong scaling performance of MBE(3)-OSV-MP2 without localization with respect to the number of GPUs (A800/80 GB). Each computing node is equipped with 8 GPUs. The parallel efficiency refers to the percentage of the actual acceleration to the ideal acceleration fold. Calculations were performed using cc-pVDZ/cc-pVDZ-RIFit basis sets for both (H₂O)₁₀₀ and (H₂O)₃₀₀ clusters.

4.3 Large Molecules

Figure 4 compares the single-GPU performance of RI-MP2 timings in ByteQC⁵⁷ and EXESS¹³ with the current MBE(3)-OSV-MP2 GPU implementation on water clusters using cc-pVDZ/cc-pVDZ-RIFit basis sets. The MBE(3)-OSV-MP2 energies are sufficiently accurate, e.g., recovering 99.97% of the RI-MP2 correlation energy for (H₂O)₃₂ as shown in see Table S1, and therefore such timing comparison is reasonable. Overall, the MBE(3)-OSV-MP2 significantly outperforms RI-MP2 due to both low-scaling algorithm and GPU parallelism which systematically exploit the locality in LMOs, OSVs and sparse fitting AOs. Compared to ByteQC’s RI-MP2, the MBE(3)-OSV-MP2 calculation achieves 2.6×, 13.1× and 40.3× accelerations for (H₂O)₄₀, (H₂O)₈₀ and (H₂O)₁₂₈, respectively. Even CPU I/O and host–device transfer costs are excluded from the EXESS’s RI-MP2 timings, the MBE(3)-OSV-MP2 is only slightly slower for (H₂O)₄₀, but yields 4.6× and 17.6× folds of acceleration for (H₂O)₈₀ and (H₂O)₁₂₈, respectively. This

indicates a substantially better GPU-based speedup scalability of MBE(3)-OSV-MP2 compared to canonical RI-MP2. Moreover, the on the fly regeneration of Γ_i in MBE(3)-OSV-MP2 avoids $N_{\text{occ}}(N_{\text{ao}} + N_{\text{vir}})N_{\text{aux}}$ storage and $N_{\text{occ}}(N_{\text{occ}} + 1)N_{\text{vir}}N_{\text{aux}}$ data movement that plague the canonical RI-MP2 GPU calculation for large molecules. This used to be an important bottleneck that limited disk I/O and host–device data transfers arising from low-bandwidth operations, which are now significantly alleviated in the present GPU algorithm.

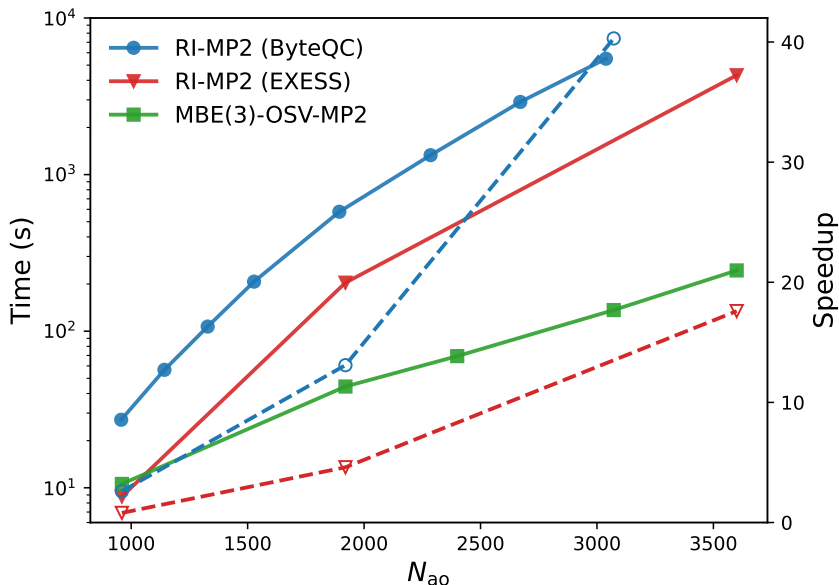


Figure 4: Wall time (seconds) comparison between GPU-accelerated MBE(3)-OSV-MP2, ByteQC’s RI-MP2,⁵⁷ as well as computational time (seconds) of EXESS’s RI-MP2.¹³ Dashed curves indicate the speedup of MBE(3)-OSV-MP2 relative to RI-MP2. RI-MP2 calculations were performed on an A100 (80 GB) GPU,^{13,57} while MBE(3)-OSV-MP2 calculations were carried out on an A800 (80 GB) GPU. For MBE(3)-OSV-MP2 calculations, the structures of water clusters were optimized using the QM-polarizable water model ChargeNN.⁷¹

Moreover, we demonstrate the GPU acceleration of MBE(3)-OSV-MP2 energy calculation compared to our previous CPU-based implementation⁸ for large molecules, as shown in Figure 5. The localization was carried out using 1 CPU core, and all subsequent steps employed 48 cores for $(\text{H}_2\text{O})_{190}/\text{cc-pVTZ}$ due to memory limitation and 64 cores for all other tested systems. In the CPU implementation, Figure 5a shows that the single-core PM localization using meta-Löwdin charges together with the co-iterative augmented Hessian (CIAH) rotation method⁷² requires even

longer time than the following parallel MBE(3)-OSV-MP2 steps for all tested systems. Switching to Löwdin charges and Jacobi optimizer, the localization step on CPU is substantially accelerated, achieving $\sim 19\times$ of speedup for $(\text{H}_2\text{O})_{190}/\text{cc-pVTZ}$. Using the same charge model and optimizer, the localization step is further expedited on GPU: about 3-fold speedup for $\text{C}_{60}@catcher$ (374 occupied orbitals) and 22–27-fold for $(\text{H}_2\text{O})_{190}$ (950 occupied orbitals). The latter speedup is substantially greater due to the larger orbital pairs that better exploit GPU parallelism with higher active thread occupancy for $(\text{H}_2\text{O})_{190}$ than $\text{C}_{60}@catcher$.

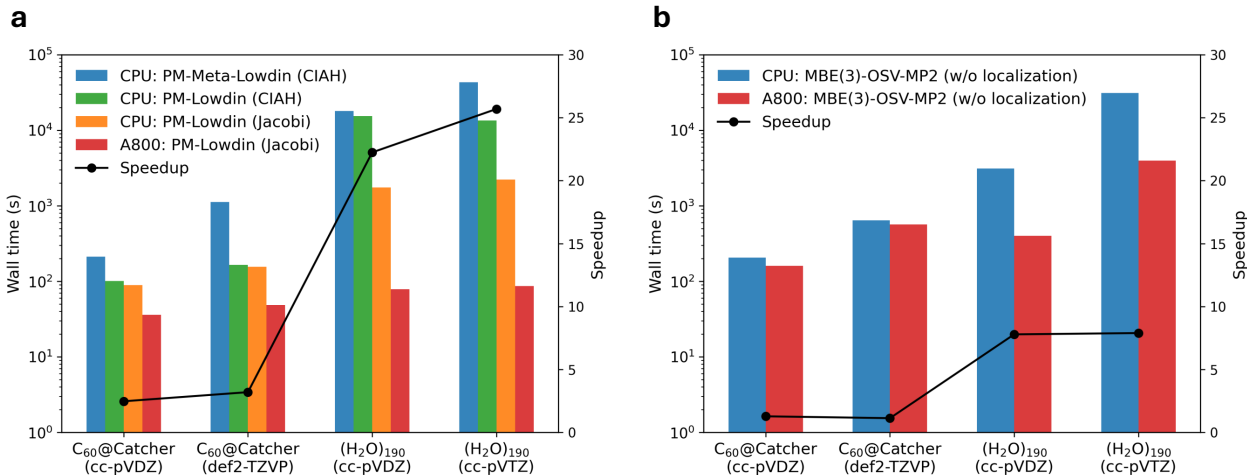


Figure 5: Wall time (seconds) for (a) localization and (b) subsequent MBE(3)-OSV-MP2 processes, measured on a single NVIDIA A800 (80 GB) GPU and 64 Intel Xeon Platinum 8360Y (2.40 GHz) CPU cores. The coordinates of $\text{C}_{60}@catcher$ and $(\text{H}_2\text{O})_{190}$ were taken from Refs. 73 and 74, respectively.

For the subsequent MBE(3)-OSV-MP2 steps after localization, only 1.1–1.3 folds of GPU acceleration is achieved for the conjugated system $\text{C}_{60}@catcher$ compared to parallel calculations on 64 CPU cores. This minor improvement stems primarily from two interrelated consequences of the extensive electron delocalization: first, the large OSV space (average 93 for $\text{C}_{60}@catcher/\text{cc-pVTZ}$) generates heavy global memory traffic, as well as restricts kernel occupancy as fewer pairs or MBE clusters can be processed in each kernel launch; second, the highly nonuniform OSV distribution (standard deviation of 41) leads to severe workload imbalance among thread blocks, each of which is assigned with calculations of an LMO pair or an MBE cluster. These factors result in residual iterations on the GPU being approximately $1.7\times$ slower than the corresponding CPU

execution. Specific workflow and kernel optimizations will be necessary to improve efficiency for systems exhibiting similarly extended and heterogeneous virtual orbital spaces.

About 8.0-fold speedup is obtained for $(\text{H}_2\text{O})_{190}$, owing to its much more compact and uniform OSV spaces (average size of 55 with a standard deviation of 7 for $(\text{H}_2\text{O})_{190}/\text{cc-pVTZ}$). In the corresponding CPU calculations, the $3c2e$ coefficient tensor Γ_i is precomputed and stored on disk, requiring 3.6 TB of storage. Although multi-process MPI parallelization enables effective overlap of I/O operations to access Γ_i with computation, pure CPU processing still accounts for only about 40% of the total elapsed time for the $(\text{H}_2\text{O})_{190}/\text{cc-pVTZ}$ system. The GPU implementation eliminates both the high storage demand and the dominant CPU I/O bottleneck by generating the Γ_i intermediates directly on the fly, thereby enabling markedly better scalability for large-scale calculations.

Overall, GPU implementation yields $1.3\times$ – $1.5\times$ accelerations for C_{60} @catcher and $8.3\times$ – $10.2\times$ for $(\text{H}_2\text{O})_{190}$ in MBE(3)-OSV-MP2 compared to CPU-only execution. Based on the hourly rate of Tianhe-2 platform, each CPU node costs 64 core hours per hour, while each A800 card consumes resources economically equivalent to 80 core hours per hour. Therefore, the GPU-accelerated calculations deliver both major timing and economic savings, along with significantly power usage, especially for localized systems like water clusters.

Finally, we showcase the performance of our multi-GPU implementation on a large biomolecule: the 784-atom human insulin peptide (a key hormone comprising 51 amino acids). Calculations were carried out using both cc-pVDZ and cc-pVTZ basis sets, together with their corresponding RIFit auxiliary basis sets, on 8 NVIDIA A800 GPUs. The memory usage and wall time are significantly reduced for all important MBE(3)-OSV-MP2 processes as summarized in Table 2. The efficient MBE(3)-OSV-MP2 computations are promoted due to the highly compact LMOs, OSVs and fitting space. The peak memory storage remains modest at 88 GB for cc-pVDZ and 241 GB for cc-pVTZ that fit well to available host memory without incurring expensive disk I/O operation. For cc-pVDZ basis ($N_{\text{ao}}=7571$, $N_{\text{aux}}=28022$), the MBE(3)-OSV-MP2 energy calculation was completed in 1429.7 s, including 406.7 s for Hartree–Fock and 1023.0 s for MP2 correlation en-

ergy (including localization). With larger cc-pVTZ basis ($N_{\text{ao}}=17448$, $N_{\text{aux}}=44319$), the total wall time rises to 6.5 hours, consisting of 1.7 hours for Hartree-Fock and 4.8 hours for MP2 correlation (including localization).

Table 2: Molecular size, memory usage (GB), and wall time (s) for MBE(3)-OSV-MP2 calculations of insulin performed on 8 NVIDIA A800 GPUs, using cc-pVDZ and cc-pVTZ basis sets with corresponding auxiliary basis sets. The structure of insulin was taken from Ref. 75.

Molecular size				
Basis set	cc-pVDZ		cc-pVTZ	
Atoms	784		784	
Occupied orbitals	1538		1538	
Orbital basis	7571		17448	
MP2 fitting basis	28022		44319	
Memory usage (GB)				
\mathbf{Q}_i	1.9		9.3	
$\tilde{\Gamma}_i^{\mu_j A'}$	77.3		196.7	
OSV S matrix	3.2		12.2	
OSV K matrix	4.1		14.5	
Max memory usage	88.0		240.6	
Wall time				
	Wall time (s)	Fraction (%)	Wall time (s)	Fraction (%)
Hartree-Fock	406.7		6226.7	
Localization	470.4	46.0	536.0	3.1
Γ_i (ERI)	125.1	12.2	11272.8	65.9
Γ_i (transformation)	332.0	32.4	4597.0	26.9
rSVD	30.7	3.0	331.6	1.9
OSV S/F	4.4	0.4	16.1	0.1
OSV K matrix	47.8	4.7	316.5	1.9
Residual iteration	12.8	1.2	37.7	0.2
MBE(3)-OSV-MP2	1023.0	100	17107.8	100
Total	1429.7		23334.5	

We further analyze the computational costs of MBE(3)-OSV-MP2 individual steps for insulin, as shown in Table 2. For cc-pVDZ basis, the localization carried out on a single GPU forms a major task as compared to other multi-GPU steps in correlation computation. It is expected that the multi-GPU localization implementation would shorten its single-GPU wall time significantly and become unimportant. The primary bottlenecks are the repeated construction of the two-electron intermediate tensor Γ_i on the fly, which accounts for 44.6% of the total time with cc-pVDZ and

increases to to 92.8% with cc-pVTZ. This strong basis-set dependence arises because the present implementation of Γ_i generation is subject to the availability of limited GPU memory: a small capacity forces excessive recomputation of the 3c2e integrals ($\alpha\beta|A$). The number of such regenerations ranges from only 13 for cc-pVDZ to 207 for cc-pVTZ on each A800 (80 GB) GPU, thereby increasing their contribution to the total wall time from 12.2% to 65.9%. The development of a Γ_i construction scheme with reduced sensitivity to memory constraints will be crucial for enabling the application of the method to substantially larger systems in future studies. In addition to the substantial speedup achieved by exploiting sparsity in the localized orbital spaces, the remaining computational steps are significantly accelerated through the use of highly optimized CUDA kernels specifically designed for the massively parallel evaluation of thousands of LMO pairs (or MBE clusters). This strategy leads to a very low overall computational overhead, amounting to only 9.3% for the cc-pVDZ basis set and 4.1% for cc-pVTZ.

5 Conclusions

In this work, we introduce a novel multi-GPU implementation to enable efficient large-scale MBE(3)-OSV-MP2 energy computation across distributed compute nodes. Key advancements include robust scaling-reduced GPU algorithms such as Jacobi-Pipek–Mezey orbital localization and randomized OSV generation. We also implemented a direct Γ_i generator to eliminate I/O bottlenecks. In addition, we engineered highly specialized CUDA kernels to maximize GPU parallel efficiency and arithmetic intensity. As a result, the GPU accelerated MBE(3)-OSV-MP2 achieves empirical sub- $\mathcal{O}(N^2)$ scalings with molecular size and 84% parallel efficiency across 24 GPUs distributed on multiple nodes. Compared to cutting-edge canonical RI-MP2 implementations, our GPU-accelerated MBE(3)-OSV-MP2 delivers 40 \times speedup in wall-clock time for the (H₂O)₁₂₈ cluster in the cc-pVDZ basis set. Relative to our previous CPU-based MBE(3)-OSV-MP2 implementation, the present GPU version provides up to 10 \times acceleration, highlighting the substantial computational gain on GPU platforms. Finally, we demonstrate the practical applicability of this

implementation to treating large biochemical systems: a full MBE(3)-OSV-MP2 energy calculation of the human insulin peptide with 784 atoms completes in only 24 minutes using cc-pVDZ basis set and in 6.4 hours with cc-pVTZ basis set.

There are several limitations in the current implementation. The GPU parallel localization has been implemented but can only function on a single GPU. In addition, the direct 3c2e generator of Γ_i heavily relies on the availability of the often short device memory, which limits the application to molecular systems consisting thousands of atoms in a single MP2 calculation without using system fragmentation. Furthermore, advanced kernel optimizations can be conducted to promote the GPU parallel efficiency, including tuning specialized variants/template pools to OSV compactness, better shared memory use for contracting intermediates with reduced bank conflicts, occupancy-aware block/grid configurations for higher warp occupancy, mixed precision, and Tensor Core acceleration at acceptable precision.

The current GPU-accelerated implementation provides a promising tool for *ab initio* calculations on large molecular systems. Future work will be extended to GPU-supported coupled-cluster model, periodic systems, MP2 analytical energy gradients and machine learning frameworks.

Acknowledgement

The authors acknowledge financial supports from the Hong Kong Research Grant Council through General Research Funds (17309020, 17310922, 17305724), the Hong Kong Quantum AI Lab through Research Talent Hub from Innovation and Technology Fund of Hong Kong Innovation and Technology Commission, and the Hung Hing Ying Physical Sciences Research Fund of the University of Hong Kong. The authors also thank the National Supercomputing Center in Guangzhou for providing high-performance computational resources. Q. L. thanks Dr. Qiming Sun for helpful discussions.

Supporting Information Available

The Supporting Information is available free of charge at

Results of correlation energy accuracy of GPU-based MBE(3)-OSV-MP2 compared to CPU implementation across various molecular systems, a list of custom kernels implemented in this work and coordinates of water clusters optimized with ChargeNN.

References

- (1) Zhang, I. Y.; Xu, X. Doubly hybrid density functional for accurate description of thermochemistry, thermochemical kinetics and nonbonded interactions. *Int. Rev. Phys. Chem.* **2011**, *30*, 115–160.
- (2) Goerigk, L.; Grimme, S. Double-hybrid density functionals. *Wiley Interdiscip. Rev. Comput. Mol. Sci.* **2014**, *4*, 576–600.
- (3) Schütz, M.; Werner, H.-J.; Lindh, R.; Manby, F. R. Analytical energy gradients for local second-order Møller–Plesset perturbation theory using density fitting approximations. *J. Chem. Phys.* **2004**, *121*, 737–750.
- (4) Lochan, R. C.; Shao, Y.; Head-Gordon, M. Quartic-Scaling Analytical Energy Gradient of Scaled Opposite-Spin Second-Order Møller–Plesset Perturbation Theory. *J. Chem. Theory Comput.* **2007**, *3*, 988–1003.
- (5) Pinski, P.; Neese, F. Communication: Exact analytical derivatives for the domain-based local pair natural orbital MP2 method (DLPNO-MP2). *J. Chem. Phys.* **2018**, *148*, 031101.
- (6) Pinski, P.; Neese, F. Analytical gradient for the domain-based local pair natural orbital second order Møller–Plesset perturbation theory method (DLPNO-MP2). *J. Chem. Phys.* **2019**, *150*, 164102.

- (7) Zhou, R.; Liang, Q.; Yang, J. Complete OSV-MP2 analytical gradient theory for molecular structure and dynamics simulations. *J. Chem. Theory Comput.* **2019**, *16*, 196–210.
- (8) Liang, Q.; Yang, J. Third-Order Many-Body Expansion of OSV-MP2 Wave Function for Low-Order Scaling Analytical Gradient Computation. *J. Chem. Theory Comput.* **2021**, *17*, 6841–6860.
- (9) Mochizuki, Y.; Yamashita, K.; Murase, T.; Nakano, T.; Fukuzawa, K.; Takematsu, K.; Watanabe, H.; Tanaka, S. Large scale FMO-MP2 calculations on a massively parallel-vector computer. *Chem. Phys. Lett.* **2008**, *457*, 396–403.
- (10) Doser, B.; Lambrecht, D. S.; Kussmann, J.; Ochsenfeld, C. Linear-scaling atomic orbital-based second-order Møller–Plesset perturbation theory by rigorous integral screening criteria. *J. Chem. Phys.* **2009**, *130*, 064107.
- (11) Nagy, P. R.; Samu, G.; Kállay, M. An integral-direct linear-scaling second-order Møller–Plesset approach. *J. Chem. Theory Comput.* **2016**, *12*, 4897–4914.
- (12) Kjærgaard, T.; Baudin, P.; Bykov, D.; Eriksen, J. J.; Ettenhuber, P.; Kristensen, K.; Larkin, J.; Liakh, D.; Pawłowski, F.; Vose, A.; others Massively parallel and linear-scaling algorithm for second-order Møller–Plesset perturbation theory applied to the study of supramolecular wires. *Comput. Phys. Commun.* **2017**, *212*, 152–160.
- (13) Snowdon, C.; Barca, G. M. An Efficient RI-MP2 Algorithm for Distributed Many-GPU Architectures. *J. Chem. Theory Comput.* **2024**, *20*, 9394–9406.
- (14) Barca, G. M.; Vallejo, J. L. G.; Poole, D. L.; Alkan, M.; Stocks, R.; Rendell, A. P.; Gordon, M. S. Enabling large-scale correlated electronic structure calculations: scaling the RI-MP2 method on summit. Proc. Int. Conf. High Perform. Comput. Netw. Storage Anal. 2021; pp 1–15.

- (15) Barca, G. M.; Snowdon, C.; Vallejo, J. L. G.; Kazemian, F.; Rendell, A. P.; Gordon, M. S. Scaling correlated fragment molecular orbital calculations on Summit. SC22: Int. Conf. High Perform. Comput. Netw. Storage Anal. 2022; pp 1–14.
- (16) Häser, M.; Almlöf, J. Laplace transform techniques in Møller–Plesset perturbation theory. *J. Chem. Phys.* **1992**, *96*, 489–494.
- (17) Schäfer, T.; Ramberger, B.; Kresse, G. Quartic scaling MP2 for solids: A highly parallelized algorithm in the plane wave basis. *J. Chem. Phys.* **2017**, *146*.
- (18) Ayala, P. Y.; Scuseria, G. E. Linear scaling second-order Møller–Plesset theory in the atomic orbital basis for large molecular systems. *J. Chem. Phys.* **1999**, *110*, 3660–3671.
- (19) Kobayashi, M.; Nakai, H. Implementation of Surján’s density matrix formulae for calculating second-order Møller–Plesset energy. *Chem. Phys. Lett.* **2006**, *420*, 250–255.
- (20) Jung, Y.; Lochan, R. C.; Dutoi, A. D.; Head-Gordon, M. Scaled opposite-spin second order Møller–Plesset correlation energy: An economical electronic structure method. *J. Chem. Phys.* **2004**, *121*, 9793–9802.
- (21) Maurer, S.; Kussmann, J.; Ochsenfeld, C. Communication: A reduced scaling J-engine based reformulation of SOS-MP2 using graphics processing units. *J. Chem. Phys.* **2014**, *141*.
- (22) Pulay, P. Localizability of dynamic electron correlation. *Chem. Phys. Lett.* **1983**, *100*, 151–154.
- (23) Kohn, W. Density functional and density matrix method scaling linearly with the number of atoms. *Phys. Rev. Lett.* **1996**, *76*, 3168–3171.
- (24) Maslen, P.; Head-Gordon, M. Non-iterative local second order Møller–Plesset theory. *Chem. Phys. Lett.* **1998**, *283*, 102–108.
- (25) El Azhary, A.; Rauhut, G.; Pulay, P.; Werner, H.-J. Analytical energy gradients for local second-order Møller–Plesset perturbation theory. *J. Chem. Phys.* **1998**, *108*, 5185–5193.

- (26) Werner, H.-J.; Manby, F. R.; Knowles, P. J. Fast linear scaling second-order Møller-Plesset perturbation theory (MP2) using local and density fitting approximations. *J. Chem. Phys.* **2003**, *118*, 8149–8160.
- (27) Yang, J.; Kurashige, Y.; Manby, F. R.; Chan, G. K. Tensor factorizations of local second-order Møller–Plesset theory. *J. Chem. Phys.* **2011**, *134*, 044123.
- (28) Werner, H.-J.; Knizia, G.; C., K.; Schwilk, M.; Dornbach, M. Scalable electron correlation methods. I. PNO–LMP2 with linear scaling in the molecular size and near–inverse–linear scaling in the number of processors. *J. Chem. Theory Comput.* **2015**, *11*, 484—507.
- (29) Pavošević, F.; Pinski, P.; Riplinger, C.; Neese, F.; Valeev, E. F. Sparse Maps-A systematic infrastructure for reduced-scaling electronic structure methods. IV. Linear-scaling second-order explicitly correlated energy with pair natural orbitals. *J. Chem. Phys.* **2016**, *144*, 144109.
- (30) Li, W.; Li, S. Divide-and-conquer local correlation approach to the correlation energy of large molecules. *J. Chem. Phys.* **2004**, *121*, 6649–6657.
- (31) Kobayashi, M.; Akama, T.; Nakai, H. Second-order Møller–Plesset perturbation energy obtained from divide-and-conquer Hartree-Fock density matrix. *J. Chem. Phys.* **2006**, *125*, 204106.
- (32) Gordon, M. S.; Fedorov, D. G.; Pruitt, S. R.; Slipchenko, L. V. Fragmentation methods: A route to accurate calculations on large systems. *Chem. Rev.* **2012**, *112*, 632–672.
- (33) Liu, K.-Y.; Herbert, J. M. Energy-screened many-body expansion: A practical yet accurate fragmentation method for quantum chemistry. *J. Chem. Theory Comput.* **2019**, *16*, 475–487.
- (34) Herbert, J. M. Fantasy versus reality in fragment-based quantum chemistry. *J. Chem. Phys.* **2019**, *151*, 170901.
- (35) Yasuda, K. Two-electron integral evaluation on the graphics processor unit. *J. of Comput. Chem.* **2008**, *29*, 334–342.

- (36) Ufimtsev, I. S.; Martinez, T. J. Quantum chemistry on graphical processing units. 1. Strategies for two-electron integral evaluation. *J. Chem. Theory Comput.* **2008**, *4*, 222–231.
- (37) Miao, Y.; Merz Jr, K. M. Acceleration of electron repulsion integral evaluation on graphics processing units via use of recurrence relations. *J. Chem. Theory Comput.* **2013**, *9*, 965–976.
- (38) Miao, Y.; Merz Jr, K. M. Acceleration of high angular momentum electron repulsion integrals and integral derivatives on graphics processing units. *J. Chem. Theory Comput.* **2015**, *11*, 1449–1462.
- (39) Barca, G. M.; Galvez-Vallejo, J. L.; Poole, D. L.; Rendell, A. P.; Gordon, M. S. High-performance, graphics processing unit-accelerated Fock build algorithm. *J. Chem. Theory Comput.* **2020**, *16*, 7232–7238.
- (40) Alkan, M.; Pham, B. Q.; Del Angel Cruz, D.; Hammond, J. R.; Barnes, T. A.; Gordon, M. S. LibERI—A portable and performant multi-GPU accelerated library for electron repulsion integrals via OpenMP offloading and standard language parallelism. *J. Chem. Phys.* **2024**, *161*.
- (41) Li, R.; Sun, Q.; Zhang, X.; Chan, G. K.-L. Introducing GPU acceleration into the python-based simulations of chemistry framework. *J. Phys. Chem. A* **2025**, *129*, 1459–1468.
- (42) Palethorpe, E.; Stocks, R.; Barca, G. M. Advanced techniques for high-performance Fock matrix construction on GPU clusters. *J. Chem. Theory Comput.* **2024**, *20*, 10424–10442.
- (43) Kalinowski, J.; Wennmohs, F.; Neese, F. Arbitrary angular momentum electron repulsion integrals with graphical processing units: Application to the resolution of identity Hartree–Fock method. *J. Chem. Theory Comput.* **2017**, *13*, 3160–3170.
- (44) Stocks, R.; Palethorpe, E.; Barca, G. M. Multi-GPU RI-HF Energies and Analytic Gradients—Toward High-Throughput Ab Initio Molecular Dynamics. *J. Chem. Theory Comput.* **2024**, *20*, 7503–7515.

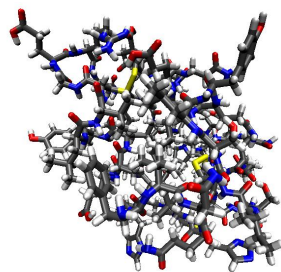
- (45) Song, C.; Martínez, T. J. Atomic orbital-based SOS-MP2 with tensor hypercontraction. I. GPU-based tensor construction and exploiting sparsity. *J. Chem. Phys.* **2016**, *144*.
- (46) Song, C.; Martínez, T. J. Atomic orbital-based SOS-MP2 with tensor hypercontraction. II. Local tensor hypercontraction. *J. Chem. Phys.* **2017**, *146*.
- (47) Asadchev, A.; Gordon, M. S. New multithreaded hybrid CPU/GPU approach to Hartree–Fock. *J. Chem. Theory Comput.* **2012**, *8*, 4166–4176.
- (48) Kussmann, J.; Ochsenfeld, C. Pre-selective screening for matrix elements in linear-scaling exact exchange calculations. *J. Chem. Phys.* **2013**, *138*.
- (49) Barca, G. M.; Alkan, M.; Galvez-Vallejo, J. L.; Poole, D. L.; Rendell, A. P.; Gordon, M. S. Faster self-consistent field (SCF) calculations on GPU clusters. *J. Chem. Theory Comput.* **2021**, *17*, 7486–7503.
- (50) Qi, J.; Zhang, Y.; Yang, M. A hybrid CPU/GPU method for Hartree–Fock self-consistent-field calculation. *J. Chem. Phys.* **2023**, *159*.
- (51) Tomlinson, D. G.; Asadchev, A.; Gordon, M. S. A new approach for second-order perturbation theory. *J. Comput. Chem.* **2016**, *37*, 1274–1282.
- (52) Pototschnig, J. V.; Papadopoulos, A.; Lyakh, D. I.; Repisky, M.; Halbert, L.; Severo Pereira Gomes, A.; Jensen, H. J. A.; Visscher, L. Implementation of relativistic coupled cluster theory for massively parallel GPU-accelerated computing architectures. *J. Chem. Theory Comput.* **2021**, *17*, 5509–5529.
- (53) Huang, Z.; Guo, Z.; Cao, C.; Pham, H. Q.; Wen, X.; Booth, G. H.; Chen, J.; Lv, D. A multi-resolution systematically improvable quantum embedding scheme for large-scale surface chemistry calculations. *Nat. Commun.* **2025**, *16*, 9297.
- (54) Vogt, L.; Olivares-Amaya, R.; Kermes, S.; Shao, Y.; Amador-Bedolla, C.; Aspuru-Guzik, A.

- Accelerating resolution-of-the-identity second-order Møller–Plesset quantum chemistry calculations with graphical processing units. *J. Phys. Chem. A* **2008**, *112*, 2049–2057.
- (55) Kwack, J.; Bertoni, C.; Pham, B.; Larkin, J. Performance of the RI-MP2 fortran kernel of GAMESS on GPUs via directive-based offloading with math libraries. Int. Workshop Accel. Program. Using Directives. 2019; pp 91–113.
- (56) Stocks, R.; Palethorpe, E.; Barca, G. M. High-performance multi-GPU analytic RI-MP2 energy gradients. *J. Chem. Theory Comput.* **2024**, *20*, 2505–2519.
- (57) Guo, Z.; Huang, Z.; Chen, Q.; Shao, J.; Liu, G.; Pham, H. Q.; Huang, Y.; Cao, C.; Chen, J.; Lv, D. ByteQC: GPU-Accelerated Quantum Chemistry Package for Large-Scale Systems. *Wiley Interdiscip. Rev. Comput. Mol. Sci.* **2025**, *15*, e70034.
- (58) Bykov, D.; Kjaergaard, T. The GPU-enabled divide-expand-consolidate RI-MP2 method (DEC-RI-MP2). *J. Comput. Chem.* **2017**, *38*, 228–237.
- (59) Pham, B. Q.; Carrington, L.; Tiwari, A.; Leang, S. S.; Alkan, M.; Bertoni, C.; Datta, D.; Sattasathuchana, T.; Xu, P.; Gordon, M. S. Porting fragmentation methods to GPUs using an OpenMP API: Offloading the resolution-of-the-identity second-order Møller–Plesset perturbation method. *J. Chem. Phys.* **2023**, *158*.
- (60) Kazemian, F. S.; Galvez Vallejo, J. L.; Barca, G. M. High-Performance, Accurate Large-Scale Quantum Chemistry Calculations on GPU Supercomputers using Coulomb-Perturbed Fragmentation. Proc. 53rd Int. Conf. Parallel Process. 2024; pp 1092–1102.
- (61) Feng, H.; Zheng, Y.; Wang, Y.; Li, S.; Li, W. Efficient Computational Strategies of the Cluster-in-Molecule Local Correlation Approach for Interaction Energies of Large Host–Guest Systems. *J. Chem. Theory Comput.* **2025**, *21*, 2998–3009.
- (62) Raffenetti, R. C.; Ruedenberg, K.; Janssen, C. L.; Schaefer, H. F. Efficient use of Jacobi rotations for orbital optimization and localization. *Theor. Chim. Acta.* **1993**, *86*, 149–165.

- (63) Wu, X.; Sun, Q.; Pu, Z.; Zheng, T.; Ma, W.; Yan, W.; Xia, Y.; Wu, Z.; Huo, M.; Li, X.; others Enhancing GPU-Acceleration in the Python-Based Simulations of Chemistry Frameworks. *Wiley Interdiscip. Rev. Comput. Mol. Sci.* **2025**, *15*, e70008.
- (64) Seritan, S.; Bannwarth, C.; Fales, B. S.; Hohenstein, E. G.; Isborn, C. M.; Kokkila-Schumacher, S. I.; Li, X.; Liu, F.; Luehr, N.; Snyder Jr, J. W.; others TeraChem: A graphical processing unit-accelerated electronic structure package for large-scale ab initio molecular dynamics. *Wiley Interdiscip. Rev. Comput. Mol. Sci.* **2021**, *11*, e1494.
- (65) Werner, H.-J.; Knowles, P. J.; Knizia, G.; Manby, F. R.; Schütz, M. Molpro: a general-purpose quantum chemistry program package. *Wiley Interdiscip. Rev. Comput. Mol. Sci.* **2012**, *2*, 242–253.
- (66) Neese, F. The ORCA program system. *Wiley Interdiscip. Rev. Comput. Mol. Sci.* **2012**, *2*, 73–78.
- (67) Furche, F.; Ahlrichs, R.; Hättig, C.; Klopper, W.; Sierka, M.; Weigend, F. Turbomole. *Wiley Interdiscip. Rev. Comput. Mol. Sci.* **2014**, *4*, 91–100.
- (68) Halko, N.; Martinsson, P.-G.; Tropp, J. A. Finding structure with randomness: Probabilistic algorithms for constructing approximate matrix decompositions. *SIAM Rev.* **2011**, *53*, 217–288.
- (69) Katouda, M.; Naruse, A.; Hirano, Y.; Nakajima, T. Massively parallel algorithm and implementation of RI-MP2 energy calculation for peta-scale many-core supercomputers. *J. Comp. Chem.* **2016**, *37*, 2623–2633.
- (70) Martínez-Martínez, L. A.; Amador-Bedolla, C. Gpu algorithm for the scaled opposite-spin (sos) mp2 energy evaluation. *J. Mex. Chem. Soc.* **2017**, *61*, 60–66.
- (71) Liang, Q.; Yang, J. Polarizable Water Model with Ab Initio Neural Network Dynamic Charges and Spontaneous Charge Transfer. *J. Chem. Theory Comput.* **2025**, *21*, 3360–3373.

- (72) Sun, Q. Co-iterative augmented Hessian method for orbital optimization. *arXiv preprint arXiv:1610.08423* **2016**,
- (73) Sure, R.; Grimme, S. Comprehensive benchmark of association (free) energies of realistic host–guest complexes. *J. Chem. Theory Comput.* **2015**, *11*, 3785–3801.
- (74) The water cluster geometries. <http://www.ergoscf.org/xyz/h2o.php>, Accessed: August 1, 2025.
- (75) Bank, R. P. D. Structure of 3I40. <https://www.rcsb.org/structure/3I40>, 2025; Accessed: August 1, 2025.

TOC Graphic



Insulin
($C_{256}H_{381}N_{65}O_{76}S_6$)

MBE(3)-OSV-MP2
(8 NVIDIA A800 GPUs)

cc-pVDZ
7571 AOs
28022 fitting AOs
HF+MP2 energy: 23.8 minutes

cc-pVTZ
17448 AOs
44319 fitting AOs
HF+MP2 energy: 6.5 hours

Supporting Information

Multi-GPU MBE(3)-OSV-MP2 for Performant Large-Scale *ab initio* Calculations

Qiujiang Liang^{†,‡} and Jun Yang^{*,†,‡,¶}

[†]*Department of Chemistry, The University of Hong Kong, Hong Kong 999077, P.R. China*

[‡]*Hong Kong Quantum AI Lab Limited, Hong Kong 999077, P.R. China*

[¶]*CAS-HKU Joint Laboratory on New Materials, The University of Hong Kong, Hong Kong 999077, P.R. China*

E-mail: juny@hku.hk

1 Accuracy

Table S1: Percentage of canonical RI-MP2 correlation energy recovered by GPU-based and CPU-based¹ MBE(3)-OSV-MP2 for various molecular systems.

	basis	N_{ao}	$E_c^{\text{MBE(3)-OSV-MP2}} / E_c^{\text{RI-MP2}}$	
			CPU ¹ (%)	GPU (%)
DIAD	def2-TZVP	1392	99.67	99.68
BHS	def2-TZVP	1586	99.80	99.81
Nonactin	def2-TZVP	1996	99.81	99.86
YIVNOG	def2-TZVP	2046	99.86	99.87
FLP	def2-TZVP	2059	99.69	99.71
(H ₂ O) ₃₂	aug-cc-pVTZ	2944	99.92	99.97

2 Algorithms

Table S2: Custom Kernels developed in this work

Steps	Kernels
Γ_i generation	sparseHalfTransKernel
Localization	pijaLowdinKernel computeRotAnglesKernel reduceAijBij1BlockKernel rotateUKernel rotatePijaRowKernel
OSV generation	normalizeVec1BlockKernel batchedDnorm2Kernel findMaxValue1BlockKernel
OSV S/F	osvSFKernel
OSV K	imujpKernel closeOsvKmatKernel remoteOsvKmatKernel
OSV Residual	closeOsvPreconKernel remoteOsvPreconKernel closeResidualKernel remoteResidualKernel clusterResidualKernel

3 Coordinates

120				H	5.088	3.640	8.430	H	10.045	7.931	8.717
w40 optimized with ChargeNN				H	5.075	2.178	8.942	H	8.752	8.310	9.485
O	6.195	6.913	7.494	O	7.645	10.542	5.463	O	0.884	6.106	2.806
H	5.771	6.046	7.335	H	7.975	9.665	5.720	H	0.686	5.171	2.863
H	5.530	7.589	7.269	H	7.769	11.077	6.266	H	1.377	6.340	3.612
O	4.614	9.046	7.007	O	2.230	4.389	6.534	O	1.984	7.541	0.779
H	4.747	9.412	6.114	H	1.650	4.543	7.296	H	1.537	7.072	1.510
H	3.673	8.795	7.077	H	2.138	5.145	5.930	H	1.440	7.424	0.000
O	5.085	7.063	3.937	O	4.609	7.556	1.372	O	9.001	1.735	7.358
H	5.162	7.986	4.238	H	3.669	7.558	1.101	H	9.669	1.119	7.661
H	4.826	7.124	2.992	H	4.925	8.472	1.307	H	8.608	2.132	8.165
O	4.857	4.626	7.051	O	9.883	4.022	6.085	O	5.370	7.186	12.056
H	3.894	4.527	6.904	H	9.447	4.025	5.216	H	4.996	6.320	11.794
H	5.258	4.390	6.191	H	9.607	3.199	6.522	H	5.699	7.079	12.951
O	2.445	6.683	4.992	O	6.467	3.013	2.139	240			
H	3.365	6.791	4.700	H	5.892	3.301	2.862	w80 optimized with ChargeNN			
H	2.297	7.287	5.740	H	6.393	3.691	1.442	O	7.663	6.995	9.251
O	5.815	4.413	4.563	O	6.330	5.392	0.732	H	7.393	6.106	8.952
H	6.782	4.344	4.449	H	5.583	6.008	0.742	H	6.921	7.599	9.062
H	5.557	5.300	4.260	H	7.009	5.801	1.286	O	5.949	9.046	8.814
O	5.274	9.741	4.467	O	0.892	4.958	8.897	H	6.170	9.394	7.929
H	5.219	9.957	3.522	H	0.000	5.101	9.215	H	5.066	8.633	8.742
H	6.128	10.112	4.765	H	1.442	5.688	9.232	O	6.140	7.515	5.431
O	8.429	8.072	6.425	O	7.922	2.844	9.517	H	6.398	8.352	5.863
H	8.768	8.482	7.246	H	6.955	2.926	9.540	H	5.449	7.780	4.789
H	7.613	7.604	6.690	H	8.292	3.707	9.781	O	6.881	4.512	8.460
O	2.134	8.074	7.371	O	8.151	10.315	2.788	H	6.120	4.825	7.937
H	2.342	7.454	8.091	H	8.757	9.568	2.894	H	7.526	4.176	7.810
H	1.734	8.836	7.827	H	8.043	10.675	3.684	O	4.807	5.788	7.169
O	8.404	4.060	3.736	O	6.726	0.916	6.050	H	5.230	6.244	6.423
H	8.375	4.943	3.332	H	6.653	1.319	5.182	H	4.397	6.488	7.710
H	7.949	3.470	3.104	H	7.569	1.212	6.435	O	7.690	5.331	5.796
O	7.681	6.576	2.900	O	10.149	6.209	7.626	H	8.617	5.595	5.934
H	8.360	7.219	3.158	H	9.563	6.690	7.025	H	7.186	6.149	5.644
H	6.840	6.872	3.284	H	10.264	5.340	7.195	O	6.805	9.918	6.416
O	9.613	8.200	3.931	O	3.741	9.110	10.844	H	6.456	10.787	6.141
H	10.542	7.959	3.907	H	4.221	8.566	11.487	H	7.766	10.054	6.502
H	9.324	8.128	4.857	H	4.435	9.568	10.331	O	9.688	8.672	8.838
O	2.800	6.772	9.709	O	4.925	0.732	8.066	H	9.468	9.390	9.464
H	2.986	7.612	10.163	H	4.330	0.000	7.906	H	8.971	8.013	8.914
H	3.399	6.118	10.113	H	5.571	0.738	7.332	O	3.683	7.674	8.753
O	7.095	7.596	9.943	O	2.484	3.168	10.380	H	3.787	7.328	9.660
H	6.689	7.198	9.147	H	1.875	3.583	9.751	H	2.841	8.157	8.718
H	6.519	7.390	10.699	H	3.249	2.844	9.878	O	10.300	6.102	6.077
O	4.351	4.945	11.063	O	5.655	10.128	1.776	H	10.215	7.014	5.745
H	4.899	4.400	10.467	H	6.611	10.171	1.979	H	10.765	5.618	5.368
H	3.563	4.377	11.170	H	5.452	10.919	1.273	O	7.925	7.539	3.271
O	5.820	9.974	9.279	O	1.565	9.950	9.288	H	8.743	7.875	3.673
H	6.355	9.203	9.535	H	1.157	10.780	9.536	H	7.246	7.618	3.963
H	5.389	9.750	8.433	H	2.264	9.767	9.938	O	9.950	8.502	4.856
O	8.142	11.043	8.080	O	8.870	5.391	9.938	H	10.772	8.767	4.402
H	7.316	10.902	8.572	H	9.437	5.576	9.169	H	9.765	9.180	5.526
H	8.802	10.454	8.477	H	8.269	6.141	10.032	O	4.343	6.584	11.158
O	5.132	3.107	9.248	O	9.435	8.665	8.892	H	3.733	6.952	11.825

H	5.101	6.206	11.642	H	5.462	2.654	11.083	H	4.920	7.913	14.917
O	8.190	7.343	11.868	O	7.746	11.934	3.841	O	6.089	12.499	6.006
H	8.030	7.323	10.907	H	8.689	12.027	4.036	H	6.188	12.661	6.960
H	7.538	6.722	12.238	H	7.257	12.312	4.591	H	5.151	12.657	5.796
O	6.416	5.337	12.439	O	3.448	12.374	8.279	O	2.568	1.282	7.118
H	6.692	4.574	11.896	H	3.274	12.542	7.340	H	3.173	0.890	7.781
H	6.695	5.138	13.349	H	4.411	12.417	8.390	H	2.578	2.237	7.291
O	6.449	10.667	10.880	O	10.549	5.998	11.889	O	5.675	10.712	2.482
H	6.266	10.331	11.777	H	11.167	6.501	11.331	H	6.410	11.187	2.915
H	6.161	9.971	10.259	H	9.741	6.539	11.939	H	6.083	10.166	1.783
O	9.153	10.736	10.439	O	9.841	9.070	13.292	O	1.902	4.994	3.957
H	8.223	10.676	10.714	H	10.532	9.469	12.736	H	2.685	4.405	3.974
H	9.303	11.691	10.277	H	9.326	8.475	12.721	H	1.633	5.138	4.873
O	7.233	3.285	10.820	O	1.921	8.928	3.434	O	9.554	2.842	4.677
H	7.095	3.658	9.924	H	1.824	8.182	2.818	H	8.634	2.877	4.367
H	7.366	2.322	10.698	H	1.597	8.617	4.301	H	10.015	3.587	4.260
O	9.457	10.357	6.821	O	3.161	11.430	3.390	O	2.105	9.673	11.137
H	9.643	9.709	7.528	H	2.620	10.625	3.317	H	2.322	10.626	11.185
H	9.732	11.213	7.203	H	4.006	11.256	2.936	H	1.845	9.503	10.221
O	2.814	3.995	7.673	O	11.400	2.956	8.706	O	7.478	0.664	10.338
H	2.870	4.009	8.646	H	11.904	2.179	8.959	H	6.885	0.000	10.696
H	3.602	4.475	7.359	H	10.895	3.190	9.510	H	7.362	0.646	9.368
O	4.569	8.555	3.627	O	6.436	7.299	15.448	O	7.549	4.804	14.863
H	3.603	8.706	3.648	H	6.881	6.458	15.258	H	8.443	4.579	14.538
H	4.954	9.374	3.251	H	7.093	8.009	15.353	H	7.292	4.086	15.444
O	12.111	5.603	8.052	O	1.267	8.991	8.534	O	9.297	13.349	9.930
H	11.405	5.812	7.410	H	0.747	9.776	8.340	H	9.691	13.375	9.041
H	11.978	4.675	8.297	H	0.640	8.273	8.755	H	8.529	13.936	9.955
O	6.915	3.454	4.033	O	11.643	9.999	11.288	O	4.778	6.756	1.588
H	7.059	4.102	4.751	H	10.767	10.286	10.973	H	3.848	6.578	1.392
H	6.948	3.975	3.210	H	11.822	9.123	10.902	H	4.744	7.321	2.382
O	7.045	5.283	2.015	O	11.585	4.789	4.097	O	11.914	9.819	3.429
H	6.180	5.633	1.732	H	11.600	4.566	3.144	H	12.416	9.012	3.658
H	7.493	6.047	2.426	H	12.069	4.084	4.567	H	11.837	9.826	2.473
O	2.950	4.398	10.357	O	6.748	8.678	0.972	O	7.955	9.587	15.081
H	2.103	4.643	10.762	H	6.036	8.025	0.895	H	8.377	10.079	15.786
H	3.551	5.136	10.566	H	7.351	8.333	1.648	H	8.663	9.384	14.434
O	9.990	3.538	10.925	O	6.313	0.897	5.071	O	0.000	6.662	9.002
H	9.019	3.455	10.881	H	5.358	0.781	4.931	H	0.268	6.221	9.825
H	10.190	4.460	11.177	H	6.560	1.728	4.636	H	0.225	6.082	8.257
O	10.506	11.838	4.780	O	5.825	10.329	13.507	O	10.634	12.685	7.566
H	11.107	11.321	4.223	H	6.606	10.116	14.047	H	10.831	12.768	6.621
H	10.078	11.198	5.366	H	5.133	9.707	13.789	H	11.440	12.365	8.014
O	8.923	2.912	7.364	O	3.419	12.942	5.558	O	4.069	3.381	4.015
H	9.113	2.922	6.408	H	3.103	13.794	5.254	H	3.857	2.456	4.233
H	9.776	2.917	7.822	H	3.281	12.327	4.807	H	5.035	3.446	4.005
O	11.814	7.520	10.008	O	12.712	7.374	4.150	O	2.375	7.579	12.741
H	11.071	7.887	9.495	H	12.360	6.491	3.957	H	2.219	8.395	12.218
H	12.214	6.868	9.413	H	13.256	7.269	4.952	H	2.926	7.853	13.494
O	6.178	12.550	8.745	O	4.493	0.587	8.878	O	14.054	6.757	6.461
H	6.429	13.343	9.248	H	5.362	0.718	8.464	H	13.411	6.360	7.073
H	6.318	11.801	9.346	H	4.476	1.108	9.700	H	14.927	6.503	6.762
O	7.007	0.958	7.697	O	0.737	5.263	6.641	O	1.994	6.627	1.859
H	6.738	0.730	6.786	H	1.497	4.767	7.011	H	1.326	6.345	1.235
H	7.631	1.695	7.586	H	0.058	4.613	6.446	H	1.956	5.997	2.612
O	4.572	2.274	11.101	O	4.134	8.437	14.664	O	12.045	2.712	5.890
H	3.945	2.979	10.868	H	3.764	8.769	15.484	H	11.203	2.421	5.503

H	11.892	2.840	6.834	O	10.808	7.301	15.050	O	9.036	13.746	2.962
O	5.370	12.864	12.059	H	11.120	7.106	14.148	H	9.890	13.542	3.374
H	5.293	12.587	12.977	H	11.297	8.102	15.305	H	8.841	13.016	2.355
H	5.738	12.081	11.611	O	9.519	12.152	6.996	O	6.781	8.987	4.904
O	11.424	4.143	1.508	H	9.739	11.916	7.917	H	6.898	9.864	5.327
H	10.506	4.064	1.182	H	9.844	13.061	6.854	H	6.175	9.133	4.152
H	11.994	4.024	0.748	O	4.289	11.053	13.546	O	7.608	1.954	13.632
O	1.292	7.910	5.905	H	3.488	10.931	13.009	H	6.795	2.463	13.476
H	1.422	8.328	6.768	H	4.570	10.181	13.865	H	7.508	1.549	14.496
H	1.072	6.981	6.077	O	13.912	5.226	12.569	O	11.962	11.239	10.573
O	8.890	3.895	0.575	H	13.089	5.712	12.755	H	11.102	11.650	10.348
H	8.238	4.425	1.068	H	14.498	5.864	12.133	H	12.601	11.963	10.459
H	8.393	3.313	0.000	O	9.195	9.587	3.615	O	12.433	4.459	6.367
O	12.620	11.571	9.134	H	9.905	9.815	4.241	H	12.027	3.727	5.870
H	13.541	11.779	9.295	H	8.415	9.361	4.150	H	12.057	4.424	7.263
H	12.308	11.072	9.909	O	8.531	9.196	9.478	O	12.087	7.317	8.618
O	3.581	0.780	4.726	H	8.024	8.476	9.064	H	11.402	7.744	8.063
H	3.126	0.026	4.352	H	7.923	9.946	9.620	H	11.844	6.379	8.678
H	3.188	0.929	5.613	O	8.032	6.612	5.705	O	7.497	5.180	10.054
O	9.882	4.049	13.727	H	8.926	6.948	5.908	H	7.386	5.844	9.343
H	10.299	4.858	13.387	H	7.561	7.343	5.273	H	7.610	4.318	9.600
H	9.883	3.456	12.961	O	8.968	8.933	12.134	O	2.781	14.645	5.239
O	0.815	5.707	11.500	H	8.870	9.150	11.189	H	2.235	15.284	4.778
H	1.317	6.407	11.960	H	8.463	8.106	12.233	H	2.915	13.900	4.623
H	0.164	5.385	12.125	O	7.197	7.101	8.226	O	14.842	5.765	6.321
O	2.795	12.273	10.950	H	6.318	7.391	7.922	H	14.010	5.266	6.236
H	3.617	12.576	11.361	H	7.669	6.883	7.400	H	15.169	5.520	7.200
H	2.908	12.376	9.987	O	7.273	15.650	10.291	O	2.465	14.347	8.007
O	6.774	14.593	10.456	H	7.626	15.258	11.107	H	2.444	14.384	7.039
H	6.300	14.097	11.150	H	7.054	16.561	10.501	H	3.377	14.553	8.267
H	6.441	15.490	10.481	O	4.937	8.277	11.081	O	13.560	3.291	10.772
300				H	4.296	8.322	11.816	H	13.692	3.880	11.546
w100 optimized with ChargeNN				H	5.764	7.938	11.468	H	14.187	3.633	10.112
O	11.836	9.813	15.357	O	0.170	8.618	9.355	O	11.031	10.316	5.497
H	11.611	10.408	16.072	H	0.447	7.958	10.016	H	11.988	10.135	5.540
H	11.512	10.217	14.534	H	0.187	8.168	8.496	H	10.758	10.679	6.364
O	4.065	14.160	11.264	O	5.093	9.689	2.892	O	13.268	13.601	10.229
H	4.744	13.625	11.707	H	4.166	9.652	3.185	H	12.514	14.148	10.531
H	4.422	14.411	10.397	H	5.302	10.644	2.829	H	14.052	14.005	10.602
O	8.556	12.358	13.669	O	13.934	12.508	5.297	O	4.502	9.778	8.833
H	8.065	11.619	14.074	H	13.906	11.534	5.370	H	4.705	9.311	9.664
H	9.390	11.945	13.387	H	14.709	12.723	4.778	H	3.564	10.046	8.897
O	3.183	12.678	3.389	O	5.091	4.287	11.010	O	14.665	5.205	9.055
H	2.920	11.763	3.574	H	4.447	4.896	10.603	H	14.938	5.897	9.683
H	4.089	12.639	3.036	H	5.953	4.529	10.631	H	13.706	5.299	8.944
O	2.154	10.686	11.857	O	5.002	3.534	4.361	O	0.626	7.388	6.897
H	1.828	11.598	11.838	H	5.096	2.747	3.825	H	1.472	6.909	7.004
H	2.201	10.465	10.912	H	5.897	3.801	4.631	H	0.000	6.763	6.530
O	11.316	12.876	4.352	O	11.846	4.638	9.097	O	3.046	6.251	7.211
H	12.268	12.932	4.523	H	12.350	3.975	9.598	H	3.203	6.136	8.168
H	11.054	11.993	4.668	H	11.100	4.851	9.686	H	3.753	6.853	6.916
O	11.115	6.059	0.895	O	15.114	7.155	10.963	O	7.147	6.947	12.099
H	10.482	6.697	1.280	H	14.341	7.750	10.914	H	7.264	6.248	11.432
H	10.765	5.856	0.026	H	15.880	7.712	11.108	H	6.884	6.514	12.932
O	5.691	12.063	8.066	O	6.107	12.587	12.335	O	12.838	8.637	10.817
H	6.186	11.851	7.252	H	6.892	12.614	12.901	H	12.588	9.575	10.797
H	5.130	11.288	8.255	H	5.454	12.030	12.811	H	12.509	8.254	9.979

H	8.370	11.504	7.657	H	13.040	8.675	8.648	H	2.618	12.441	10.872
H	7.558	10.872	6.509	H	13.716	7.662	9.598	H	2.117	11.039	10.357
O	7.235	7.400	9.871	O	7.925	6.915	5.397	O	13.300	13.053	11.462
H	6.739	8.211	9.670	H	8.142	7.246	6.287	H	12.637	13.753	11.309
H	7.823	7.299	9.101	H	8.451	7.462	4.789	H	14.151	13.395	11.129
O	6.033	9.626	8.798	O	9.129	8.702	3.745	O	13.036	7.714	4.963
H	6.712	9.949	8.186	H	8.646	9.263	3.112	H	12.937	8.274	4.177
H	5.876	10.350	9.440	H	9.610	9.297	4.349	H	13.989	7.603	5.127
O	8.848	7.954	7.743	O	3.374	8.007	12.047	O	9.218	12.123	4.050
H	9.819	7.862	7.808	H	2.435	7.813	11.885	H	8.308	11.880	4.296
H	8.665	8.903	7.658	H	3.394	8.863	12.513	H	9.789	11.534	4.576
O	8.744	13.222	7.805	O	11.531	6.361	12.193	O	7.640	4.315	6.322
H	8.452	13.743	7.035	H	10.597	6.437	11.915	H	6.667	4.233	6.367
H	9.710	13.364	7.831	H	11.510	5.789	12.983	H	7.812	5.217	6.003
O	11.704	11.815	9.557	O	12.444	13.473	4.904	O	7.210	13.949	14.375
H	12.034	12.510	10.156	H	13.027	12.703	4.787	H	8.000	13.618	14.838
H	10.945	11.420	10.026	H	12.068	13.396	5.800	H	6.473	13.499	14.816
O	5.548	11.484	10.620	O	11.016	5.011	8.761	O	4.901	15.499	7.322
H	5.780	10.852	11.330	H	11.210	5.321	7.857	H	3.940	15.419	7.208
H	4.584	11.612	10.670	H	11.718	5.366	9.324	H	5.274	14.969	6.598
O	11.580	7.979	7.659	O	13.632	10.253	11.431	O	15.985	9.677	5.821
H	11.805	8.848	7.279	H	13.310	11.155	11.254	H	15.907	8.716	5.702
H	11.827	7.314	6.990	H	13.607	9.769	10.584	H	16.173	9.808	6.764
O	10.286	10.297	5.640	O	7.057	16.495	11.113	O	5.867	4.450	10.166
H	11.136	10.382	6.110	H	7.569	17.277	11.395	H	6.743	4.385	9.737
H	9.594	10.372	6.321	H	7.636	15.744	11.335	H	5.948	5.128	10.861
O	12.365	10.507	7.297	O	8.364	4.187	8.942	O	1.852	8.398	7.562
H	13.170	10.946	6.964	H	8.121	4.144	7.996	H	2.686	8.388	8.067
H	12.132	10.986	8.117	H	9.264	4.560	8.966	H	1.700	7.462	7.330
O	6.451	9.615	12.307	O	5.747	6.499	12.066	O	7.458	10.670	16.049
H	5.968	9.509	13.147	H	4.899	6.972	12.130	H	7.854	9.782	16.040
H	7.375	9.373	12.491	H	6.299	7.023	11.459	H	8.202	11.282	15.913
O	10.739	11.608	13.537	O	8.661	14.447	5.375	O	7.023	16.947	8.355
H	10.390	11.329	12.673	H	9.163	13.749	4.917	H	6.977	16.793	9.314
H	10.700	10.825	14.123	H	9.194	15.263	5.347	H	6.271	16.474	7.954
O	9.005	8.835	12.880	O	4.815	15.179	10.055	O	3.729	5.382	8.842
H	9.025	7.957	12.450	H	4.865	15.279	9.088	H	4.409	4.898	9.351
H	8.963	8.663	13.836	H	5.554	15.675	10.439	H	3.919	6.326	9.000
O	8.661	14.481	12.104	O	12.952	8.364	13.241	O	7.205	14.716	3.076
H	8.167	14.253	12.912	H	13.057	9.074	12.582	H	7.703	14.509	3.889
H	8.399	13.796	11.456	H	12.361	7.696	12.845	H	7.699	15.478	2.726
O	11.160	14.450	10.701	O	12.999	12.848	14.168	O	3.725	6.358	4.777
H	10.303	14.491	11.153	H	13.289	13.091	13.271	H	4.487	6.109	4.226
H	11.426	15.367	10.503	H	12.187	12.324	14.005	H	3.676	7.325	4.699
O	8.933	6.410	11.706	O	4.037	11.666	4.761	O	11.897	5.623	6.229
H	8.365	6.653	10.951	H	3.917	10.738	4.492	H	11.804	4.724	5.845
H	8.691	5.491	11.940	H	3.243	11.892	5.278	H	12.218	6.195	5.510
O	11.415	13.635	7.505	O	5.452	14.006	5.077	O	3.234	10.488	13.291
H	11.640	13.030	8.234	H	4.790	13.346	4.801	H	3.026	11.202	13.923
H	11.849	14.484	7.715	H	5.886	14.354	4.280	H	3.107	10.893	12.413
O	3.906	8.054	9.312	O	13.293	5.991	10.214	O	8.479	3.862	12.506
H	3.765	8.140	10.273	H	13.966	5.499	10.710	H	8.499	3.930	13.474
H	4.667	8.621	9.086	H	12.615	6.206	10.883	H	9.241	3.296	12.259
O	6.749	11.629	5.198	O	9.321	12.770	15.554	O	8.605	8.105	15.553
H	5.904	11.223	4.950	H	9.828	12.200	14.943	H	9.344	7.568	15.902
H	6.494	12.563	5.330	H	9.938	13.480	15.786	H	7.926	7.464	15.277
O	13.764	8.586	9.298	O	2.847	11.491	10.815	O	12.083	16.942	10.106

H	12.443	16.662	9.242	H	2.652	14.439	12.108	H	7.107	8.525	1.458
H	11.467	17.670	9.930	H	3.429	14.508	10.765	H	7.390	7.060	1.029
O	7.954	10.034	1.619	O	9.028	18.157	11.962	O	14.608	12.064	7.108
H	8.691	9.907	0.987	H	9.589	17.611	12.538	H	15.187	11.434	7.574
H	7.679	10.959	1.531	H	9.570	18.448	11.214	H	14.653	11.831	6.165
O	13.955	11.073	4.651	O	6.843	6.220	14.614	O	10.660	2.424	12.038
H	14.750	10.550	4.871	H	6.561	6.246	13.679	H	11.598	2.648	12.073
H	13.447	10.511	4.044	H	6.034	6.425	15.124	H	10.449	2.098	11.140
O	11.423	14.618	15.538	O	10.052	16.800	5.333	O	11.685	3.134	5.418
H	11.942	15.051	16.218	H	11.017	16.685	5.376	H	10.811	2.898	5.058
H	12.037	14.035	15.050	H	9.782	17.367	6.074	H	11.769	2.677	6.276
O	0.899	9.851	9.703	O	0.080	12.030	8.168	O	9.548	1.744	9.644
H	0.727	9.170	10.369	H	0.183	12.886	8.626	H	9.051	2.553	9.424
H	1.222	9.372	8.919	H	0.244	11.325	8.814	H	8.880	1.062	9.841
O	12.896	15.949	7.767	O	10.982	7.025	16.213	O	14.788	11.108	15.247
H	12.901	16.197	6.828	H	11.157	6.247	15.657	H	15.303	11.591	15.895
H	13.761	15.510	7.927	H	11.814	7.524	16.262	H	14.143	11.742	14.877
O	6.149	6.071	3.530	O	8.638	4.273	15.197	O	15.602	6.965	5.685
H	6.241	6.712	2.803	H	7.997	5.000	15.072	H	15.217	6.498	6.454
H	6.737	6.381	4.248	H	8.239	3.658	15.815	H	16.018	6.291	5.146
O	5.252	9.436	14.753	O	11.515	14.674	2.561	O	10.440	16.165	13.425
H	4.514	9.958	14.384	H	11.843	14.243	3.365	H	10.662	15.750	14.270
H	5.845	10.029	15.242	H	11.044	13.985	2.064	H	9.867	15.533	12.962
O	15.945	10.147	8.572	O	13.107	16.350	12.558	O	12.208	11.194	0.711
H	15.237	9.558	8.894	H	12.903	16.634	11.649	H	11.514	11.807	1.020
H	16.341	10.573	9.347	H	12.246	16.313	13.003	H	12.733	11.670	0.066
O	3.568	9.058	4.117	O	1.088	5.534	9.654	O	6.338	2.250	11.762
H	2.629	9.190	4.335	H	0.699	5.451	8.776	H	5.950	2.904	11.156
H	3.642	8.892	3.159	H	2.037	5.369	9.522	H	7.109	2.701	12.142
O	14.282	5.589	7.597	O	15.436	7.265	13.044	O	15.679	15.508	12.795
H	13.448	5.437	7.117	H	14.516	7.524	13.230	H	14.739	15.778	12.763
H	14.035	5.690	8.527	H	15.907	8.108	12.965	H	16.185	16.317	12.868
O	5.589	16.026	13.466	O	13.098	8.878	15.851	O	9.294	16.393	2.678
H	6.199	15.375	13.849	H	13.114	8.617	14.909	H	10.084	15.877	2.444
H	5.984	16.311	12.627	H	13.728	9.607	15.914	H	9.476	16.755	3.559
O	12.697	9.346	2.724	O	1.122	9.597	5.247	O	0.833	14.461	9.150
H	12.084	8.650	2.429	H	1.361	9.211	6.114	H	1.398	14.397	9.940
H	12.664	10.014	2.022	H	0.207	9.360	5.092	H	1.407	14.716	8.412
O	1.651	12.192	6.038	O	15.874	10.042	12.897	O	1.901	5.790	6.800
H	1.116	12.163	6.858	H	15.044	10.085	12.380	H	2.374	5.880	5.955
H	1.396	11.376	5.583	H	15.640	10.382	13.775	H	2.564	5.464	7.431
O	10.740	7.500	1.939	O	5.595	12.630	16.206	O	2.263	14.830	6.715
H	10.174	7.806	2.672	H	5.558	12.978	17.099	H	2.131	13.897	6.465
H	10.258	6.765	1.537	H	6.218	11.882	16.227	H	1.634	15.340	6.202
O	15.111	14.560	8.138	O	8.926	18.420	7.290	O	4.014	8.356	1.512
H	15.425	14.376	9.039	H	8.411	19.052	6.785	H	4.957	8.134	1.421
H	14.977	13.695	7.713	H	8.266	17.804	7.677	H	3.564	7.971	0.759
O	4.944	4.535	6.494	O	11.717	2.374	8.077	O	7.357	12.784	1.164
H	4.516	5.135	5.861	H	11.012	1.865	8.509	H	7.233	13.435	1.882
H	4.566	4.728	7.366	H	11.569	3.289	8.361	H	6.818	13.088	0.431
O	11.287	4.865	14.464	O	15.162	4.859	11.896	O	10.605	9.977	15.592
H	11.846	4.161	14.096	H	15.298	5.697	12.387	H	9.985	9.241	15.713
H	10.409	4.484	14.635	H	16.013	4.635	11.514	H	11.485	9.604	15.780
O	0.731	7.587	11.349	O	10.083	12.602	1.545	O	17.130	11.322	10.877
H	0.000	7.377	11.932	H	9.218	12.774	1.145	H	16.711	10.843	11.618
H	0.830	6.825	10.743	H	9.872	12.372	2.470	H	18.073	11.170	10.947
O	2.623	14.142	11.185	O	6.686	7.653	1.336	O	7.379	0.223	10.271

H	6.710	0.000	9.625	H	11.107	13.937	9.242	H	12.816	6.372	14.990
H	6.971	0.849	10.900	O	13.471	12.099	10.616	O	13.843	14.561	6.813
O	8.767	5.802	0.842	H	13.881	12.486	11.410	H	14.447	13.843	6.564
H	8.943	5.378	0.000	H	12.742	11.540	10.950	H	13.598	14.371	7.740
H	8.430	5.108	1.439	O	7.197	11.519	12.033	O	11.814	6.192	10.401
O	15.794	13.783	10.695	H	7.344	11.022	12.863	H	12.174	6.185	9.496
H	15.914	14.372	11.464	H	6.254	11.756	12.041	H	12.570	6.106	10.997
H	16.356	13.002	10.816	O	13.408	9.129	8.678	O	15.177	10.541	13.208
O	10.135	9.453	0.108	H	13.500	10.067	8.427	H	14.904	11.469	13.123
H	10.849	10.101	0.216	H	13.755	8.616	7.926	H	14.846	10.069	12.422
H	10.401	8.671	0.623	O	11.715	11.280	6.190	O	8.488	16.581	12.491
O	7.510	3.991	2.432	H	12.472	11.461	6.775	H	8.822	17.491	12.600
H	6.980	4.643	2.930	H	10.917	11.533	6.690	H	9.181	15.979	12.834
H	6.978	3.195	2.376	O	13.760	11.700	7.957	O	9.444	4.735	10.297
O	3.054	15.147	13.724	H	14.706	11.538	7.786	H	9.192	4.749	9.351
H	2.525	15.891	14.015	H	13.680	11.964	8.896	H	10.299	5.194	10.358
H	3.970	15.479	13.629	O	7.562	10.066	14.256	O	7.668	6.176	14.059
O	10.307	18.977	9.584	H	7.032	10.209	15.062	H	7.087	6.915	13.797
H	10.468	19.920	9.545	H	8.485	9.955	14.560	H	8.578	6.446	13.834
H	9.807	18.740	8.783	O	12.081	10.607	14.335	O	11.031	14.989	6.941
O	3.137	12.651	14.902	H	11.959	10.628	13.370	H	11.959	14.719	7.008
H	3.974	12.686	15.389	H	11.308	10.123	14.679	H	11.043	15.962	6.876
H	3.027	13.514	14.469	O	9.996	8.948	14.929	O	6.024	15.431	11.889
O	9.082	2.835	4.531	H	10.035	8.176	14.342	H	6.078	15.360	10.923
H	8.603	3.235	5.279	H	9.932	8.608	15.841	H	6.866	15.805	12.193
H	8.741	3.255	3.733	O	10.195	14.741	13.431	O	14.324	8.967	15.348
O	13.182	3.300	13.080	H	9.872	14.652	14.344	H	14.385	9.684	14.692
H	13.643	2.545	13.449	H	9.984	13.901	12.978	H	13.687	8.332	14.976
H	13.846	3.849	12.633	O	12.653	15.071	12.270	O	13.334	12.718	15.354
O	4.529	7.004	15.737	H	11.772	14.941	12.667	H	13.784	13.029	14.553
H	3.674	6.771	15.375	H	12.761	16.031	12.158	H	12.853	11.911	15.070
H	4.717	7.918	15.455	O	10.217	6.692	13.349	O	5.508	11.198	7.450
O	12.743	16.203	5.054	H	10.194	7.095	12.455	H	5.280	10.739	6.627
H	13.102	16.569	4.244	H	10.297	5.723	13.239	H	4.701	11.629	7.781
H	12.688	15.239	4.912	O	12.884	14.420	9.309	O	6.979	13.390	7.541
450				H	13.078	13.691	9.924	H	6.417	12.590	7.612
w150 optimized with ChargeNN				H	13.154	15.235	9.771	H	7.818	13.076	7.164
O	11.458	10.624	11.662	O	5.793	8.233	10.353	O	14.224	6.431	12.097
H	10.990	9.783	11.506	H	5.947	8.285	11.317	H	15.022	6.125	12.565
H	10.767	11.304	11.787	H	6.538	8.726	9.969	H	13.617	6.674	12.823
O	9.640	12.605	11.897	O	8.957	12.318	5.948	O	9.276	11.880	15.908
H	9.759	12.993	11.009	H	8.369	11.930	5.276	H	10.021	11.711	16.514
H	8.719	12.282	11.951	H	9.198	13.199	5.599	H	9.269	12.835	15.736
O	9.702	11.277	8.280	O	14.677	8.947	11.073	O	4.459	11.708	12.270
H	9.919	12.094	8.771	H	14.098	9.043	10.294	H	3.972	12.426	11.832
H	9.228	11.568	7.482	H	14.516	8.050	11.415	H	3.942	10.903	12.095
O	9.976	8.310	11.231	O	9.939	7.126	6.640	O	14.474	13.222	12.887
H	9.193	8.749	10.853	H	10.156	7.597	7.469	H	13.860	13.964	12.704
H	10.472	7.967	10.463	H	10.348	7.669	5.948	H	15.378	13.585	12.812
O	7.990	9.846	10.051	O	10.673	9.125	4.903	O	14.434	7.911	6.474
H	8.460	10.323	9.349	H	9.984	9.587	4.394	H	14.376	8.165	5.539
H	7.715	10.510	10.712	H	11.101	9.816	5.441	H	15.383	7.974	6.689
O	10.734	8.738	8.610	O	6.184	8.175	13.007	O	11.465	11.926	3.541
H	11.704	8.817	8.663	H	5.291	8.149	13.401	H	10.520	11.722	3.429
H	10.386	9.638	8.482	H	6.663	8.914	13.435	H	11.639	11.762	4.486
O	10.211	13.633	9.476	O	12.754	7.016	14.258	O	8.632	4.898	7.722
H	9.669	14.444	9.475	H	11.816	7.043	14.001	H	7.669	5.061	7.779

H	9.044	5.690	7.336	H	3.044	9.104	10.949	H	1.801	12.716	10.892
O	9.013	14.657	15.912	O	14.145	16.835	9.937	O	12.271	7.195	18.168
H	9.774	14.639	16.516	H	14.060	17.161	9.026	H	12.718	6.577	17.570
H	8.206	14.490	16.441	H	15.104	16.797	10.127	H	12.706	8.063	18.088
O	6.205	15.406	9.130	O	7.696	7.277	5.206	O	10.481	3.915	16.461
H	5.265	15.542	8.910	H	7.999	7.503	4.310	H	9.731	4.529	16.581
H	6.470	14.624	8.608	H	8.495	7.204	5.762	H	10.259	3.121	16.948
O	16.326	10.806	7.597	O	5.809	10.216	16.345	O	13.550	15.489	4.202
H	16.556	9.959	7.173	H	5.166	10.827	15.937	H	13.615	15.153	5.110
H	16.596	10.673	8.522	H	6.315	10.733	17.001	H	13.596	14.723	3.611
O	7.212	4.723	11.754	O	17.024	9.796	10.003	O	14.476	17.107	14.251
H	8.021	4.738	11.200	H	16.195	9.658	10.499	H	13.921	17.414	13.514
H	7.384	5.303	12.520	H	17.304	8.898	9.745	H	13.875	16.824	14.958
O	3.296	8.552	9.311	O	4.901	9.999	4.994	O	3.707	5.395	13.232
H	4.256	8.491	9.475	H	3.935	10.138	5.013	H	4.241	4.774	13.759
H	2.979	7.631	9.235	H	5.089	9.437	4.216	H	4.074	5.385	12.333
O	7.447	11.665	17.867	O	15.249	5.834	9.611	O	16.761	7.759	15.294
H	7.874	11.081	18.516	H	14.496	5.989	9.008	H	15.889	8.149	15.498
H	8.094	11.718	17.135	H	14.886	5.910	10.509	H	17.228	8.427	14.765
O	8.762	15.889	9.878	O	7.501	16.881	15.070	O	13.171	9.793	17.680
H	8.698	16.137	10.818	H	7.931	16.120	15.495	H	13.469	9.532	16.788
H	7.849	15.718	9.585	H	7.802	16.874	14.147	H	13.786	10.501	17.938
O	4.972	5.658	10.652	O	14.800	8.744	3.864	O	1.832	10.530	8.208
H	5.731	5.153	11.003	H	13.940	8.463	3.499	H	2.380	9.784	8.524
H	5.272	6.587	10.636	H	14.878	9.701	3.725	H	1.289	10.778	8.972
O	9.241	14.803	4.974	O	3.418	12.756	8.372	O	17.687	9.517	13.393
H	9.791	14.931	5.772	H	3.314	12.903	9.330	H	16.773	9.851	13.310
H	9.686	15.381	4.327	H	2.776	12.060	8.152	H	18.238	10.321	13.394
O	5.318	7.582	6.368	O	12.306	7.907	3.160	O	6.653	14.185	17.116
H	6.227	7.505	6.011	H	11.744	8.303	3.855	H	5.778	14.207	16.696
H	5.053	8.490	6.161	H	11.867	7.074	2.929	H	6.764	13.304	17.515
O	13.125	6.012	7.986	O	16.767	16.694	10.589	O	9.435	18.175	8.548
H	12.968	5.154	7.543	H	16.887	16.749	11.550	H	8.561	18.359	8.164
H	13.448	6.623	7.305	H	17.174	15.862	10.294	H	9.325	17.308	8.977
O	4.136	11.827	15.014	O	5.954	5.451	8.010	O	11.896	1.924	8.627
H	4.118	12.759	15.301	H	5.661	6.231	7.510	H	10.995	1.882	9.005
H	4.296	11.847	14.053	H	5.583	5.518	8.903	H	12.494	1.935	9.389
O	10.312	3.981	13.705	O	12.939	5.178	16.224	O	16.452	5.794	13.542
H	10.470	3.919	14.661	H	13.602	4.627	15.778	H	16.523	6.440	14.280
H	11.117	3.626	13.275	H	12.130	4.646	16.315	H	17.142	6.073	12.921
O	9.793	7.772	17.362	O	3.649	8.004	13.903	O	13.499	13.269	2.490
H	10.679	7.529	17.707	H	2.994	8.440	14.480	H	13.241	13.623	1.637
H	9.309	6.945	17.210	H	3.402	7.064	13.771	H	12.699	12.851	2.865
O	12.862	17.821	12.077	O	3.735	16.618	12.674	O	8.459	7.520	2.584
H	13.449	17.573	11.339	H	3.954	17.004	13.536	H	8.764	8.192	1.955
H	12.148	18.320	11.634	H	4.563	16.188	12.378	H	9.140	6.829	2.597
O	9.030	10.718	3.309	O	11.420	18.195	14.442	O	17.479	14.565	7.177
H	8.974	10.290	2.439	H	11.724	17.570	15.118	H	17.743	15.248	6.561
H	8.144	11.073	3.507	H	12.015	18.095	13.679	H	16.894	13.955	6.696
O	15.819	12.789	5.881	O	8.316	5.530	16.644	O	12.765	3.215	12.857
H	16.081	12.054	6.467	H	7.998	5.710	15.737	H	13.530	3.423	13.413
H	15.640	12.387	5.018	H	7.561	5.709	17.231	H	13.099	2.795	12.046
O	11.511	13.959	16.918	O	11.220	17.679	6.564	O	12.890	3.606	6.838
H	11.342	13.272	17.586	H	12.119	17.776	6.913	H	12.360	3.662	6.031
H	12.147	13.532	16.309	H	10.602	17.995	7.251	H	12.433	2.963	7.425
O	2.781	9.552	11.777	O	2.605	13.256	10.979	O	9.666	1.940	10.109
H	3.044	8.970	12.512	H	2.366	14.186	10.775	H	9.522	2.882	10.293

O	6.882	23.259	10.809	O	9.815	16.601	13.180	O	19.124	5.210	12.618
H	7.424	23.553	11.555	H	10.035	16.611	12.228	H	18.533	4.937	13.340
H	6.050	22.915	11.181	H	9.393	15.738	13.355	H	18.561	5.285	11.831
O	20.510	10.459	9.508	O	16.056	12.752	19.855	O	13.261	13.661	8.461
H	21.267	11.037	9.697	H	15.970	12.628	18.892	H	14.044	14.002	8.928
H	20.357	9.979	10.345	H	15.811	13.682	20.007	H	12.486	14.084	8.869
O	12.815	17.846	18.519	O	16.278	25.380	9.621	O	2.619	12.050	18.328
H	13.080	18.048	19.433	H	16.356	24.810	8.840	H	2.881	12.703	19.010
H	13.401	17.125	18.217	H	16.888	25.001	10.275	H	1.876	11.567	18.691
O	13.638	16.288	2.920	O	20.223	5.946	9.072	O	12.869	14.308	14.305
H	13.196	16.544	3.753	H	20.301	6.792	8.597	H	12.222	13.735	13.852
H	13.368	15.368	2.724	H	20.834	5.967	9.828	H	12.427	15.162	14.478
O	8.381	17.176	8.804	O	14.435	17.552	10.717	O	12.487	5.839	6.387
H	7.981	16.285	8.789	H	14.441	16.940	11.471	H	11.613	6.227	6.573
H	9.020	17.216	8.068	H	14.765	18.411	11.049	H	12.404	4.900	6.647
O	13.107	13.638	2.682	O	6.460	15.358	22.989	O	11.873	11.886	10.710
H	13.619	12.815	2.694	H	7.426	15.420	23.095	H	12.838	11.959	10.870
H	12.395	13.503	3.328	H	6.252	14.472	22.656	H	11.649	12.644	10.145
O	2.718	21.212	13.605	O	14.658	8.563	21.604	O	16.438	14.402	23.997
H	3.312	20.556	14.014	H	15.573	8.621	21.925	H	16.679	13.481	23.797
H	2.152	21.553	14.296	H	14.561	9.313	20.983	H	16.043	14.380	24.889
O	3.436	16.294	19.575	O	15.820	1.108	11.096	O	2.937	8.662	8.531
H	3.270	17.235	19.392	H	16.395	0.377	10.870	H	2.472	8.973	9.331
H	3.408	15.912	18.679	H	15.414	0.905	11.959	H	2.726	9.296	7.817
O	20.275	11.045	20.565	O	22.028	15.683	9.667	O	12.863	13.528	16.892
H	20.885	11.465	19.939	H	21.555	15.135	10.323	H	12.855	13.759	15.941
H	19.694	11.743	20.911	H	21.585	16.546	9.677	H	12.252	12.771	16.980
O	17.436	18.963	5.544	O	7.052	19.132	22.224	O	9.403	16.924	2.663
H	17.678	18.828	4.601	H	6.984	19.002	23.170	H	10.254	17.344	2.441
H	16.574	18.509	5.640	H	6.424	18.508	21.816	H	8.821	17.081	1.917
O	9.999	6.864	6.993	O	2.068	9.627	10.944	O	11.038	12.688	13.175
H	10.199	7.814	7.072	H	2.298	9.050	11.694	H	10.187	13.163	13.225
H	9.029	6.808	6.934	H	1.888	10.503	11.315	H	11.192	12.436	12.244
O	5.836	15.209	16.225	O	5.316	8.531	9.668	O	7.551	7.867	4.533
H	6.027	16.137	16.461	H	4.451	8.531	9.207	H	7.456	7.597	5.470
H	6.000	15.080	15.274	H	5.293	7.733	10.226	H	7.499	7.058	4.023
O	12.603	17.586	5.167	O	7.621	16.870	19.490	O	11.198	20.525	14.811
H	13.475	17.603	5.602	H	6.875	16.955	20.119	H	11.731	20.315	15.600
H	12.479	18.462	4.762	H	7.894	15.937	19.524	H	11.748	21.124	14.275
O	16.122	17.299	8.613	O	17.617	10.925	17.598	O	4.538	19.650	10.219
H	16.951	16.870	8.890	H	16.697	11.225	17.495	H	3.767	19.066	10.302
H	15.507	17.255	9.368	H	18.153	11.714	17.398	H	4.514	20.037	9.321
O	12.170	3.603	7.781	O	10.166	13.053	24.183	O	14.268	5.678	8.496
H	12.615	2.874	8.248	H	9.404	12.553	24.476	H	13.611	5.706	7.772
H	11.399	3.852	8.319	H	10.359	12.778	23.267	H	13.929	5.022	9.130
O	14.317	10.385	5.897	O	7.102	3.495	15.311	O	11.106	21.960	10.159
H	13.534	10.740	6.355	H	7.841	3.491	15.950	H	10.997	22.637	10.850
H	14.177	9.424	5.778	H	6.819	2.582	15.226	H	10.508	21.245	10.443
O	9.589	26.432	13.256	O	5.822	16.967	6.569	O	8.919	13.043	16.225
H	9.388	27.154	12.660	H	6.053	17.854	6.250	H	8.183	13.134	16.863
H	10.559	26.389	13.325	H	5.174	17.084	7.286	H	9.650	12.599	16.689
O	15.531	17.940	1.811	O	12.806	2.649	13.038	O	11.301	17.380	21.913
H	14.875	17.349	2.216	H	12.154	3.119	13.585	H	12.100	17.861	21.635
H	15.265	18.069	0.900	H	12.956	3.208	12.255	H	10.557	17.872	21.519
O	8.263	9.155	20.819	O	5.152	11.067	18.034	O	2.906	10.242	6.333
H	7.815	8.290	20.896	H	4.233	11.348	18.195	H	3.521	10.016	5.620
H	9.208	8.950	20.924	H	5.682	11.888	18.012	H	3.061	11.171	6.569

O	9.241	15.556	23.203	O	7.540	14.836	6.130	O	15.216	17.519	6.059
H	9.689	14.812	23.633	H	6.956	15.614	6.168	H	15.395	17.374	7.006
H	9.914	16.180	22.905	H	6.974	14.059	6.290	H	15.391	16.667	5.609
O	4.489	12.288	13.200	O	21.952	18.200	17.874	O	4.923	16.481	12.539
H	4.608	11.739	13.998	H	22.473	18.979	18.083	H	5.448	17.292	12.666
H	4.812	11.763	12.444	H	21.847	17.694	18.696	H	4.002	16.687	12.783
O	3.500	13.636	20.328	O	16.446	5.195	6.737	O	10.904	14.226	9.658
H	3.433	14.595	20.169	H	17.091	4.559	7.092	H	10.785	15.097	10.084
H	4.277	13.491	20.890	H	15.669	5.185	7.317	H	10.532	14.334	8.754
O	14.497	3.431	17.289	O	15.083	14.201	26.350	O	17.407	19.641	8.204
H	13.621	3.055	17.066	H	14.937	14.916	26.970	H	17.523	19.561	7.242
H	14.643	4.191	16.694	H	14.210	13.939	26.007	H	17.032	18.785	8.480
O	10.026	14.669	7.226	O	5.084	9.340	4.647	O	24.477	11.240	12.255
H	9.131	14.609	6.848	H	5.501	10.213	4.752	H	25.410	11.081	12.108
H	10.322	15.584	7.057	H	5.819	8.743	4.458	H	24.182	10.557	12.891
O	18.329	6.877	18.721	O	13.736	18.499	20.997	O	12.005	2.535	16.784
H	17.889	6.174	19.229	H	14.645	18.155	21.035	H	11.825	2.914	15.907
H	18.335	7.682	19.268	H	13.827	19.461	20.873	H	11.150	2.588	17.232
O	6.477	10.343	7.796	O	16.167	9.458	13.520	O	18.632	16.829	19.215
H	5.925	9.697	8.267	H	16.911	9.359	14.141	H	18.740	15.863	19.156
H	7.359	10.289	8.205	H	15.403	9.655	14.100	H	17.831	17.007	19.738
O	1.967	12.280	12.157	O	18.610	13.334	16.816	O	12.194	7.526	17.655
H	2.803	12.225	12.657	H	17.789	13.555	16.336	H	11.266	7.825	17.639
H	1.468	12.994	12.580	H	19.287	13.875	16.373	H	12.355	7.172	18.546
O	18.674	21.353	14.584	O	19.300	15.996	2.603	O	15.842	16.489	15.579
H	18.466	21.145	15.509	H	19.434	15.486	3.420	H	15.255	17.007	14.998
H	18.268	22.222	14.405	H	19.114	15.364	1.907	H	16.744	16.831	15.426
O	8.084	7.927	9.548	O	8.999	10.203	4.631	O	17.639	8.544	11.408
H	8.348	8.854	9.388	H	9.720	10.292	3.988	H	17.100	8.012	10.799
H	7.217	7.961	9.990	H	8.562	9.344	4.484	H	17.103	8.726	12.200
O	18.779	16.666	9.002	O	18.331	12.888	21.299	O	19.297	18.575	17.223
H	18.590	15.761	9.321	H	18.051	12.561	22.171	H	18.984	17.973	17.922
H	18.992	16.604	8.054	H	17.508	12.815	20.779	H	20.268	18.540	17.271
O	9.385	9.069	14.954	O	3.440	12.841	7.273	O	16.102	12.269	13.221
H	8.690	9.751	14.886	H	3.312	13.704	6.841	H	15.464	12.326	12.484
H	10.226	9.542	14.818	H	3.271	12.935	8.229	H	16.146	11.319	13.429
O	23.833	17.787	15.783	O	11.296	21.054	6.081	O	21.083	17.124	20.319
H	23.125	17.651	16.426	H	11.748	20.868	6.925	H	20.995	17.774	21.020
H	23.981	16.958	15.298	H	10.342	21.015	6.249	H	20.202	17.025	19.911
O	10.389	9.609	6.922	O	3.250	15.596	16.927	O	20.985	14.041	11.526
H	9.879	9.850	6.127	H	3.014	16.423	16.467	H	20.088	13.737	11.756
H	11.137	10.230	6.959	H	4.179	15.410	16.696	H	21.479	13.247	11.247
O	24.208	16.074	11.403	O	8.670	23.020	17.747	O	17.748	20.831	17.205
H	23.551	15.747	10.771	H	8.808	22.177	18.218	H	18.302	20.031	17.233
H	24.104	17.040	11.394	H	7.729	23.058	17.499	H	16.874	20.568	16.852
O	9.225	18.692	20.704	O	4.625	7.444	6.689	O	5.547	17.092	21.166
H	8.772	18.012	20.168	H	4.576	8.104	5.977	H	4.742	16.809	20.697
H	8.536	18.991	21.330	H	3.947	7.703	7.336	H	5.723	16.430	21.867
O	8.682	5.785	18.221	O	2.735	17.860	15.465	O	13.532	8.402	2.517
H	7.743	5.954	18.020	H	3.433	18.467	15.158	H	12.728	8.521	2.004
H	9.148	6.606	17.982	H	2.359	17.480	14.655	H	13.888	9.292	2.688
O	8.512	21.283	6.379	O	13.963	7.799	5.196	O	23.884	12.864	14.420
H	8.468	22.170	6.016	H	13.760	7.793	4.244	H	23.791	12.248	15.168
H	8.251	21.367	7.318	H	13.466	7.062	5.601	H	24.101	12.316	13.646
O	16.842	23.219	7.893	O	10.525	17.023	17.351	O	11.612	10.566	14.718
H	16.942	22.881	6.988	H	11.289	17.409	17.818	H	11.431	11.365	14.184
H	17.575	22.837	8.407	H	10.408	16.145	17.753	H	11.792	9.863	14.058

O	11.394	9.076	0.774	O	14.067	21.174	20.428	O	19.337	17.075	6.339
H	11.892	9.352	0.000	H	13.353	21.441	19.822	H	20.144	17.492	6.030
H	10.951	8.255	0.552	H	14.146	21.879	21.074	H	18.611	17.641	6.021
O	7.299	6.626	20.507	O	19.581	11.000	13.729	O	6.600	11.613	4.955
H	6.539	6.655	19.908	H	20.181	11.584	14.230	H	7.485	11.230	4.834
H	7.987	6.181	19.986	H	19.061	10.493	14.377	H	6.491	11.760	5.912
O	17.829	5.405	10.143	O	5.313	10.979	10.941	O	2.234	16.776	12.939
H	17.209	6.108	9.883	H	6.246	10.940	11.217	H	2.066	17.120	12.047
H	18.698	5.668	9.779	H	5.125	10.110	10.542	H	1.764	15.928	13.037
O	7.189	19.162	10.232	O	7.781	10.795	12.070	O	14.090	11.701	23.769
H	6.224	19.245	10.112	H	7.819	11.079	13.003	H	13.614	12.401	24.250
H	7.492	18.417	9.677	H	8.217	11.487	11.541	H	13.456	10.998	23.571
O	20.209	9.192	11.862	O	20.972	21.242	13.015	O	23.724	9.696	14.294
H	19.341	8.780	11.698	H	21.640	20.672	13.445	H	23.319	9.995	15.124
H	20.041	9.885	12.527	H	20.216	21.298	13.622	H	23.166	8.984	13.930
O	6.586	18.650	12.875	O	6.119	22.943	16.751	O	19.758	17.689	12.682
H	6.731	18.934	11.955	H	5.292	23.262	17.117	H	20.450	17.108	13.046
H	7.442	18.756	13.323	H	6.051	23.073	15.781	H	20.032	17.843	11.767
O	18.107	9.405	15.415	O	14.030	11.015	3.254	O	7.241	7.017	7.067
H	17.980	9.972	16.200	H	14.948	11.101	2.913	H	6.266	7.026	6.972
H	18.788	8.745	15.680	H	14.159	10.881	4.214	H	7.401	7.327	7.976
O	18.542	21.731	9.532	O	11.049	11.617	17.219	O	5.012	13.724	4.010
H	19.403	21.468	9.891	H	11.228	10.989	16.496	H	5.561	14.031	3.269
H	18.154	20.922	9.154	H	11.172	11.150	18.066	H	5.439	12.912	4.330
O	3.926	5.361	12.955	O	16.883	4.819	19.825	O	22.524	12.047	10.462
H	4.547	5.628	12.248	H	15.914	4.793	19.834	H	22.884	12.506	9.684
H	3.270	4.798	12.542	H	17.175	4.019	19.383	H	23.266	11.766	11.024
O	20.725	18.181	10.101	O	17.476	23.658	16.882	O	10.083	5.004	9.084
H	20.617	19.149	10.071	H	17.749	22.751	17.085	H	10.366	5.624	9.775
H	19.932	17.797	9.680	H	17.624	23.806	15.933	H	9.938	5.549	8.293
O	15.278	14.514	10.078	O	16.440	13.861	15.362	O	12.428	20.002	3.891
H	16.245	14.451	9.964	H	16.183	14.796	15.263	H	11.930	20.429	4.617
H	15.124	14.990	10.916	H	16.257	13.409	14.515	H	13.215	20.533	3.759
O	2.978	8.043	13.068	O	14.375	20.356	13.684	O	23.016	13.572	8.225
H	3.112	7.091	12.970	H	14.849	20.281	12.831	H	22.632	14.376	8.623
H	3.690	8.344	13.652	H	13.721	21.065	13.570	H	23.800	13.850	7.751
O	16.988	4.297	14.125	O	14.100	17.707	13.963	O	7.695	11.134	14.738
H	16.594	4.112	13.253	H	13.213	17.512	14.321	H	6.757	11.046	15.000
H	16.937	3.460	14.622	H	14.167	18.677	13.883	H	8.062	11.875	15.254
O	8.140	11.889	21.171	O	17.259	9.094	22.290	O	12.581	6.264	15.166
H	8.105	10.936	20.972	H	17.890	8.552	22.766	H	12.346	6.747	15.974
H	9.064	12.070	21.417	H	17.629	9.224	21.395	H	13.508	5.984	15.292
O	19.480	14.174	19.190	O	12.547	24.020	8.963	O	16.037	7.395	9.519
H	19.007	13.695	19.894	H	12.735	23.799	8.050	H	15.366	6.797	9.126
H	19.111	13.865	18.339	H	11.990	23.309	9.324	H	16.416	7.887	8.762
O	18.348	17.267	15.036	O	21.576	15.836	13.467	O	5.307	5.601	15.367
H	18.692	17.877	15.714	H	21.454	15.200	12.738	H	4.694	5.440	14.628
H	18.732	17.540	14.182	H	22.535	15.865	13.652	H	5.957	4.880	15.334
O	8.846	14.171	13.774	O	16.688	7.416	5.252	O	16.856	11.187	6.534
H	8.897	13.879	14.704	H	16.723	6.514	5.629	H	15.919	10.977	6.364
H	7.891	14.210	13.578	H	15.739	7.593	5.119	H	17.111	11.792	5.813
O	12.952	6.856	20.236	O	9.261	6.977	13.265	O	22.108	6.711	15.544
H	13.656	7.370	20.670	H	9.811	7.155	12.479	H	22.139	7.044	14.631
H	13.315	5.966	20.099	H	9.488	7.654	13.930	H	22.981	6.823	15.920
O	11.286	10.698	3.072	O	3.469	18.608	18.135	O	12.788	24.386	15.412
H	11.160	10.281	2.210	H	4.399	18.422	17.927	H	12.113	24.374	16.110
H	12.253	10.742	3.192	H	2.983	18.478	17.307	H	13.605	24.067	15.848

O	10.954	8.541	21.182	O	16.690	20.309	19.796	O	15.496	19.958	11.320
H	11.497	7.823	20.812	H	17.075	20.598	18.950	H	15.470	20.521	10.528
H	11.406	8.820	21.997	H	15.830	20.746	19.889	H	16.425	19.922	11.634
O	6.127	6.688	17.894	O	12.642	9.278	23.254	O	13.381	14.356	5.833
H	5.718	6.376	17.072	H	12.692	8.785	24.074	H	12.585	13.971	5.436
H	6.296	7.642	17.802	H	13.409	9.005	22.714	H	13.362	14.138	6.780
O	19.697	7.629	16.433	O	9.487	20.124	11.342	O	5.099	10.775	15.340
H	19.447	7.212	17.274	H	9.405	19.861	12.271	H	5.015	10.872	16.306
H	20.524	7.210	16.134	H	8.692	19.794	10.894	H	5.063	9.817	15.151
O	12.020	14.877	21.061	O	22.857	19.484	13.862	O	14.422	8.485	11.523
H	11.679	15.729	21.389	H	23.234	18.983	14.607	H	14.951	8.065	10.825
H	12.916	14.801	21.442	H	23.124	19.025	13.054	H	15.048	8.876	12.154
O	7.019	14.150	2.131	O	19.927	15.151	22.180	O	15.135	5.531	15.665
H	7.153	13.318	1.678	H	19.495	14.352	21.841	H	15.612	6.260	16.100
H	7.778	14.280	2.725	H	20.408	15.570	21.453	H	15.783	5.121	15.059
O	17.989	14.268	9.906	O	15.267	20.429	16.227	O	17.446	23.707	14.075
H	18.141	13.500	9.318	H	15.116	20.392	15.264	H	17.880	23.916	13.231
H	18.212	13.945	10.797	H	14.402	20.222	16.620	H	16.511	23.637	13.828
O	10.386	16.706	10.574	O	16.463	17.788	20.761	O	6.123	12.906	7.380
H	9.595	16.932	10.048	H	16.894	17.580	21.619	H	5.147	12.957	7.317
H	11.102	17.255	10.200	H	16.672	18.716	20.535	H	6.295	11.996	7.700
O	6.403	20.231	16.549	O	5.318	8.220	14.607	O	16.177	3.778	11.579
H	6.328	21.187	16.694	H	5.299	7.316	14.965	H	16.785	4.236	10.973
H	7.352	20.014	16.538	H	5.926	8.202	13.845	H	16.161	2.836	11.326
O	17.347	8.674	7.496	O	5.867	23.183	14.098	O	9.389	22.590	15.123
H	17.142	8.146	6.694	H	5.382	22.737	13.381	H	9.971	21.814	15.060
H	17.153	9.596	7.243	H	6.692	23.513	13.701	H	9.157	22.711	16.058
O	12.631	20.608	8.434	O	8.311	24.019	13.125	O	5.726	6.260	11.141
H	13.563	20.853	8.573	H	8.561	24.946	13.293	H	6.365	5.582	10.837
H	12.107	21.108	9.091	H	8.669	23.496	13.871	H	6.227	6.865	11.720
O	11.027	4.021	14.688	O	12.101	5.707	12.510	O	17.950	18.339	3.059
H	10.313	4.100	14.026	H	12.336	6.193	13.320	H	18.493	17.557	2.843
H	11.528	4.860	14.650	H	11.513	6.287	11.999	H	17.117	18.237	2.563
O	2.282	17.916	10.307	O	18.420	12.008	8.577	O	12.694	20.078	17.034
H	1.533	18.377	9.924	H	19.196	11.438	8.720	H	12.700	19.232	17.518
H	2.699	17.410	9.584	H	17.971	11.713	7.761	H	12.452	20.759	17.688
O	8.393	14.222	19.615	O	10.830	23.783	12.096	O	11.905	21.894	18.899
H	8.362	13.491	20.254	H	9.900	23.829	12.390	H	11.763	22.746	18.451
H	9.313	14.289	19.303	H	11.222	24.647	12.320	H	11.025	21.479	18.975
O	21.546	5.577	11.544	O	10.733	12.543	21.576	O	10.396	7.207	10.777
H	20.681	5.467	11.994	H	11.116	11.888	20.965	H	9.536	7.404	10.355
H	21.988	4.730	11.613	H	11.186	13.383	21.375	H	11.011	7.863	10.397
O	24.169	15.596	14.098	O	21.171	12.839	14.856	O	10.925	14.626	18.618
H	24.427	15.739	13.168	H	20.801	13.704	15.102	H	11.395	14.746	19.465
H	24.243	14.643	14.270	H	22.069	13.017	14.520	H	11.521	14.118	18.044
O	12.763	16.190	23.986	O	13.906	25.335	10.956	O	9.360	3.549	16.839
H	13.481	15.913	23.391	H	14.742	25.574	10.507	H	9.210	4.312	17.428
H	12.165	16.733	23.454	H	13.359	24.928	10.256	H	9.914	3.856	16.100
O	5.090	20.674	7.771	O	16.198	2.044	15.457	O	9.113	14.550	3.917
H	5.412	20.194	6.995	H	15.647	1.543	14.834	H	9.294	15.434	3.538
H	5.851	21.182	8.103	H	15.619	2.382	16.161	H	8.563	14.694	4.710
O	9.579	8.263	17.494	O	16.772	11.711	23.246	O	7.022	8.207	12.478
H	9.501	8.458	16.540	H	16.995	10.799	23.016	H	7.831	7.774	12.815
H	8.794	8.680	17.893	H	15.809	11.700	23.411	H	7.260	9.142	12.327
O	11.237	13.008	4.615	O	12.258	18.044	9.194	O	18.259	9.302	3.926
H	11.077	12.203	4.092	H	13.080	17.813	9.663	H	18.884	9.638	4.583
H	10.455	13.577	4.476	H	12.355	18.982	8.938	H	17.737	8.595	4.344

O	14.473	14.990	22.216	O	11.984	8.748	12.853	O	18.544	13.049	12.292
H	15.129	14.697	22.875	H	11.694	8.925	11.939	H	17.622	12.965	12.591
H	14.984	15.188	21.414	H	12.929	8.559	12.742	H	18.980	12.284	12.707
O	12.676	13.717	25.102	O	22.690	11.266	16.447	O	14.341	10.585	19.889
H	11.765	13.415	24.972	H	21.951	11.691	15.978	H	14.483	10.160	19.021
H	12.700	14.617	24.722	H	22.588	11.536	17.369	H	14.936	11.356	19.930
O	20.038	8.422	7.801	O	6.173	14.379	13.616	O	8.871	10.404	9.012
H	19.065	8.427	7.715	H	5.747	15.132	13.167	H	9.567	10.283	8.339
H	20.257	9.106	8.460	H	5.565	13.622	13.505	H	9.019	11.246	9.474
O	16.601	10.823	10.220	O	18.284	9.395	19.821	O	12.257	25.895	13.097
H	17.228	11.252	9.611	H	19.110	9.854	20.069	H	12.942	25.844	12.402
H	17.054	10.050	10.596	H	17.948	9.887	19.051	H	12.632	25.521	13.914
O	10.654	17.278	7.125	O	4.654	19.547	14.585	O	14.268	10.207	15.177
H	11.253	17.569	7.838	H	5.203	19.838	15.336	H	13.325	10.381	15.024
H	11.177	17.368	6.309	H	5.285	19.258	13.904	H	14.344	9.880	16.092
O	7.171	9.259	18.299	O	14.662	15.506	12.562	O	17.624	23.661	11.357
H	7.423	9.314	19.239	H	14.677	16.285	13.146	H	16.714	23.416	11.602
H	6.459	9.911	18.167	H	14.059	14.894	13.015	H	17.972	22.949	10.796
O	12.674	22.453	13.548	O	12.075	9.213	10.189	O	18.437	3.740	8.013
H	12.721	23.123	14.263	H	11.963	10.179	10.236	H	18.177	4.130	8.859
H	12.021	22.812	12.916	H	13.006	9.028	10.400	H	19.279	4.150	7.792
O	20.076	15.222	15.563	O	8.737	4.334	13.226	O	7.728	4.534	10.608
H	20.709	15.526	14.886	H	8.840	5.305	13.245	H	8.135	4.282	11.452
H	19.344	15.857	15.483	H	8.046	4.103	13.868	H	8.452	4.600	9.962
O	17.326	13.138	4.665	O	14.120	4.401	19.753	O	14.485	12.141	11.073
H	16.677	13.865	4.653	H	14.209	4.094	18.828	H	14.686	12.998	10.651
H	18.197	13.568	4.719	H	13.791	3.647	20.246	H	15.149	11.521	10.705
O	6.718	13.230	17.769	O	13.606	4.267	10.858	O	11.772	16.706	14.950
H	6.303	13.954	17.258	H	13.085	4.891	11.399	H	11.353	16.829	15.821
H	7.177	13.645	18.522	H	14.514	4.254	11.216	H	11.043	16.707	14.298
O	4.809	15.177	10.162	O	15.352	12.429	17.302	O	6.042	17.644	17.370
H	4.822	15.571	11.054	H	15.758	12.937	16.572	H	6.609	17.443	18.137
H	4.325	14.328	10.218	H	14.406	12.632	17.230	H	6.314	18.520	17.049
O	8.736	12.771	10.432	O	12.117	11.679	6.905	O	15.091	23.464	12.500
H	9.594	13.201	10.279	H	11.766	12.222	6.176	H	14.687	24.174	11.962
H	8.085	13.392	10.056	H	12.517	12.302	7.537	H	14.348	22.969	12.876
O	5.702	12.904	21.925	O	9.134	19.066	13.927	O	7.258	14.681	9.179
H	6.525	12.542	21.557	H	9.916	19.603	14.162	H	7.032	14.228	8.343
H	5.342	12.240	22.515	H	9.463	18.173	13.698	H	6.404	14.874	9.607
O	3.608	16.656	8.285	O	14.291	15.784	17.650	O	13.511	1.888	9.509
H	3.365	16.120	7.511	H	14.863	16.035	16.897	H	14.329	1.457	9.772
H	4.067	16.059	8.909	H	13.797	14.994	17.372	H	13.439	2.676	10.072
O	3.518	12.839	10.014	O	22.209	7.788	13.023	O	9.487	20.629	18.788
H	4.179	12.152	10.226	H	22.167	6.979	12.487	H	9.288	20.051	18.028
H	2.791	12.674	10.644	H	21.494	8.344	12.660	H	9.387	20.056	19.571
O	16.623	11.211	2.815	O	14.423	9.076	17.643	O	23.310	18.663	11.182
H	16.928	11.946	3.374	H	15.177	8.501	17.413	H	22.401	18.603	10.846
H	17.196	10.455	3.046	H	13.632	8.504	17.630	H	23.650	19.517	10.915
O	16.522	7.570	16.817	O	1.826	13.508	16.009	O	15.559	15.234	4.633
H	17.153	7.236	17.484	H	2.033	12.800	16.636	H	15.144	15.556	3.815
H	17.060	8.117	16.219	H	2.292	14.291	16.362	H	14.824	14.806	5.120
O	17.877	19.733	12.511	O	6.527	19.492	5.682	O	0.949	14.401	13.631
H	18.150	20.344	13.219	H	6.381	19.644	4.747	H	0.000	14.371	13.765
H	18.504	18.993	12.539	H	7.340	19.973	5.918	H	1.340	14.081	14.473
O	3.782	15.209	5.905	O	15.262	21.220	8.867	O	11.654	10.747	19.744
H	4.540	15.814	5.933	H	15.913	20.585	8.523	H	12.627	10.718	19.821
H	3.978	14.639	5.137	H	15.625	22.091	8.623	H	11.327	9.926	20.154

O	21.834	12.637	18.861
H	21.088	13.260	18.833
H	22.530	13.069	19.361
O	17.198	21.760	5.502
H	17.431	22.056	4.622
H	17.276	20.793	5.505
O	11.095	24.243	17.671
H	10.182	23.907	17.605
H	11.049	25.063	18.166
O	19.598	14.633	4.969
H	20.207	13.981	5.366
H	19.482	15.348	5.613
O	11.769	18.119	1.948
H	12.450	17.456	2.145
H	11.927	18.864	2.550
O	20.497	10.098	5.656
H	21.093	9.665	5.041
H	20.368	9.486	6.403
O	14.592	0.754	13.535
H	13.931	1.462	13.374
H	14.096	0.000	13.856

References

- (1) Liang, Q.; Yang, J. Third-Order Many-Body Expansion of OSV-MP2 Wave Function for Low-Order Scaling Analytical Gradient Computation. *J. Chem. Theory Comput.* **2021**, *17*, 6841–6860.